UNIVERSITY OF OSLO
Department of Informatics

LC VCO tuning with parallel MOS-varactor in FDSM application

Master thesis

M. Ali Saber

1st August 2006

Acknowledgements

First, I would like to thank my family for supporting me throughout this time period, specially my mother for here encouragement and inspiration.
I am grateful to my supervisor Dag T. Wisland for sharing his knowledge and helping me grow as a student.
I would like to thank Yngvar Berg for admitting me to the professional degree program. I have enjoyed working with my fellow students Ehsan Arshad, Bjørn Christian Paulseth, Haakon Andre Hjortland, Haavard Moen, Alf Storm, Andrei Olsen and the rest of the MES group at UiO.
I also want to show appreciations to Morten Furuholmen and all others that have encouraged me along the way.

Contents

List of Figures

List of Tables

1 Introduction

Technology improvement and market growth, mainly in the communication sector, has in the last years been pushing for higher quality of service in transmission and reception of information. The conversion from real-world analog information signals into digital representation has made possible digital processing with high resolution, severely reduced noise and easy storage of the information.
Increasing user demands, has pushed the technology development into producing communication devices that are increasingly user friendly, with low-cost, compact size and low power operation.
As wireless mobile devices are battery operated, the ever increasing integration of what used to be stand-alone devices, such as cameras and radios, into single multi-functional electronic devices, has further pushed the need for low power operation.

Voltage controlled oscillators (VCO) are found in systems that require a source of variable frequency used for frequency synthesis, clock and data recovery and other applications. For instance, most radio frequency (RF) systems, contain an oscillator which generates the periodic output signal used to modulate the transmitted or received signal. In the past years there has been a lot of study on the VCOs used in RF transmission, resulting in improved overall performance.

A less known application where the VCO is used to generate frequencies, is in the frequency Delta-Sigma modulator (FDSM) system. The FDSM technique was developed at the University of Oslo (UiO), and is based on the more familiar bit stream generating Delta-Sigma ($\Delta - \Sigma$) modulator that make up the core of the $\Delta - \Sigma$ A/D converter [1]. The $\Delta - \Sigma$ converters outperform the more traditional Nyquist rate converters in situations where high resolution and low signal bandwidths are needed.
The motivation for the $\Delta - \Sigma$ converter is the awareness that in the conversion process, speed is less expensive than precision, so by using faster signal processing one can obtain higher precision. Due to noise shaping, where the spectre is shaped to push noise components out to frequencies far from the carrier, a low resolution A/D converter may be used without reducing the overall signal-to-quantization-noise ratio (SQNR).
For the FDSM, the analog state received is first converted by an oscillator, from an amplitude value into a time-domain continuous frequency variation. As the frequency coded state still remains analog, the signal-to-noise ratio is not

strongly affected by the power supply.
In order to improve the FDSM performance, it is important to have a linear relation between the input and output of the oscillator being used. The frequency modulation (FM) to digital transition in the FDSM is surprisingly modular and simple. The quantization in FDSM modulators is performed on the phase of the signal, therefore the phase noise and quantization noise are equivalent, and are both first order noise shaped. The benefits obtained from the FDSM approach is compatibility with technological scaling and low power supply operation.

1.1 Motivation

Usually, an ideal VCO would be one that is able to meet all of the specification in Table 1.

Table 1.1: Oscillator specifications.

1	low noise
2	low power
3	wide tuning range
4	integrated
5	smal die area occupancy
6	low cost

In addition, limitations in the applied semi-conductor technology should be taken into consideration.
Common benefits from using cost-effective CMOS implementation include leveraging high-volume fabrication and the potential for achieving high-levels of RF/ analog/ digital integration.
The power supply voltage V_{dd}, of CMOS devices has been steadily reduced with the scaling of device feature size, contributing to lower power requirements. This is due to higher doping levels in silicon, that reduces the resistive losses, resulting in VCOs with lower power consumption and also lower phase-noise. Also, the high off state impedance of the MOSFETs minimizes the current consumption. Based on the features just described, two major benefits arise from using the CMOS technology, one is power reduction, the other is on-chip functionality, leading to low power operation and user friendly products.

The ring oscillator is categorized as a waveform oscillator. It displays advantages such as wide tuning range, high integration in VLSI, and small die area occupancy. Usually, the ring oscillator generates lower frequencies than the LC-tank VCO, which reduces the need of an large prescaler or frequency dividers, that take up space and contribute noise of their own. Generating a reasonable low frequency for the FDSM system is important, due to the sam-

pling rate that is used in order to obtain high resolution.
At a given power consumption, LC-tank (inductance, capacitance) oscillators achieve lower phase noise than the ring oscillators, so for monolithic integration in CMOS technology, LC-tank VCOs are often preferred.
One obvious disadvantage from using an LC-tank VCO, is that it contains an inductor and often a variable capacitor, which are large area components, and therefore not well suited for VLSI implementation. In addition, its tuning range is known to be small.
So why is the LC VCO further explored in this thesis?
The LC-tank VCOs phase noise characteristics at low power supplies are superior to that of the ring oscillators, and this is a factor that is becoming increasingly important as the technology is being further downscaled [2].
The frequency tuning characteristics of the ring oscillator display an fairly linear behaviour for the applied tuning and the resulting output frequency [3]. However, this linearity suffers as the phase noise becomes more and more dominating with lower power supplies.

For the LC-tank oscillator, the frequency tuning curve is shown in Figure 1.1,

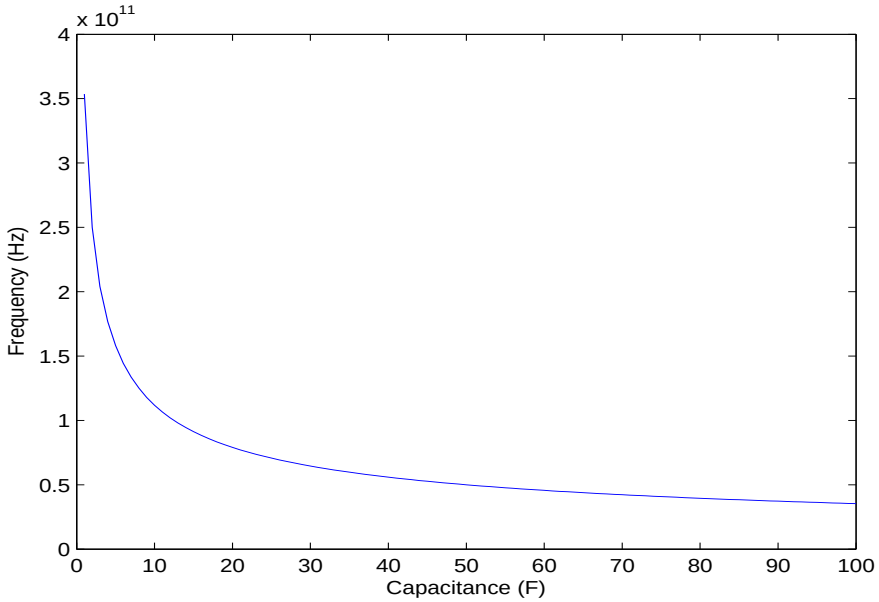

Figure 1.1: LC-tank VCOs frequency tuning curve: $\omega_{osc} = 1/\sqrt{LC}$.

and is given by:

$$\omega_{osc} = \frac{1}{\sqrt{LC(V)}}, \tag{1.1}$$

which clearly displays a systematic nonlinear characteristic, due to the inverse square law (ISL) variation. The V in Equation (1.1), represents the tuning voltage. The *C* in the expression is a term consisting of several capacitance contributing factors, but in this work, it is mainly used to represent the varactor capacitance.

To make sure the data being handled in FDSM system is not corrupted, the linearity relation between the analog input, and the digital output should be kept the highest possible.
When a LC-tank VCO is used to generate frequencies that follow an ISL-frequency behaviour, one particular solution is provided for the FDSM system that can improve the linearity. Applying digital correction at the FDSM output, essentially a squaring of the output bits, will result in a straight line.
However, this is only true if the output frequency follows the inverse square law tuning to a high degree, which is not always the case.

This thesis will focus on the LC-tank VCOs tuning characteristics, that differ from the ideal in Figure 1.1, with the main focus being on the variable MOS-capacitors.
The digital correction will be performed by another student at UiO, Ehsan Arshad, and the frequency curves resulting from this work will be analyzed.

Varactors, variable reactors, or voltage controlled capacitors, are extensively used as tuneable elements in LC-tank VCOs, and their capacitance characteristics define the output frequency of the oscillator. Nonlinearities in varactor capacitance tuning characteristics, makes it difficult for the LC-tank VCOs output frequency to perform according to the inverse square law.
Also, large amplitude swings at the LC-tank VCOs output impact the effective capacitance of the varactor, modulating the output frequency and making it hard to predict.
When a varactor with abrupt capacitance characteristics is used in an LC-tank VCO, and the oscillator amplitude swing is applied directly across it, the frequency curve shows strong dependence on the bias current (I_{bias}).
The bias current and the oscillation sustaining active elements also introduce distortion and corrupt the output frequency curve, by the up conversion of various noise sources to the resonance frequency.
Parasitic capacitances from the tank inductor, the wiring and gate to source and drain overlap capacitances are other factors that severely reduce the available capacitance tuning ranges, and therefore the frequency tuning range.

1.2 Overview of this thesis

- **Chapter two** starts of by briefly explaining the basics of the LC-tank VCOs operation. The ideal oscillator time- and frequency- domain behaviour is shown, and factors that impact the amplitude, the phase and therefore the frequency of the generated waveforms are mentioned. The mechanisms that allow oscillator to operate as they do, are mentioned, with focus on the start-up and oscillation sustaining criteria. From there two common LC-tank VCO topologies are shown, with brief explanations given as to what make them attractive/unattractive. Important trade offs, and modes of operation are mentioned, and so are some of the measurements used to make sure the oscillator work according to plan.

- **Chapter three** gives an introduction to the capacitor by briefly explaining what it is, and how its used as a variable tuning element. The benefits obtained using MOS-varactors are mentioned, and detailed explanations are given as to how they operate in different capacitance regions. Two well known MOS-varactors the AMOS and the IMOS and their capacitance tuning characteristics are shown. From there, MOS-varactor capacitance tuning characteristics, and their influence on the oscillator output frequency, are explained. Issues such as effective capacitance, tuning sensitivity, linearity, frequency range and AM-FM modulation, are mentioned. Towards the end, one way of influencing the MOS-varactors capacitance characteristics is shown, where differential gate doping is used, before this chapter ends by briefly mentioning the switched capacitance tuning method.

- **Chapter four**, this is where the design and the analysis of the MOS-varactors used in the LC-tank VCO are performed. Small adjustments are made in order to get the LC-tank VCO going and steadily oscillating, and from there the focus is shifted towards the MOS-varactor itself, with different small-signal test circuits being used to display its characteristics. The influence of the amplitude swing, frequency characteristics, phase noise and linearity in the IMOS and the so called NBG-varactors, are matters that are discussed. Simulations and curve fitting tools are applied, and used to measure and collect data. Also, the derivative of the capacitance tuning curve is used to show the fast and slow changing parts of the MOS-varactor capacitance curve. This chapter prepares for the next chapter, in which the linearity and other frequency tuning issues are further handled, with a different varactor tuning technique.

- **Chapter five**, Varactor combinations is an approach to the LC-tank VCO where more than one varactor is utilized to determine the output frequency. By combining and adjusting two or more varactors, in this case the IMOS and the so called NDSB varactor, still using one source of tun-

ing voltage, improvement in varactor linearity and in some parts a wider frequency tuning range is shown. The potential for zero AM-FM modulation over a wide tuning range is illustrated, and some important trade offs are mentioned. In addition, phase noise improvements are shown, demonstrating the potential of the combined varactor structure.

2 The LC-tank VCO

The frequency domain characteristics of an ideal oscillator, consisting of an Dirac impulse at the centre frequency ω_o, is illustrated in Figure 2.1a.
The ideal oscillator would be one that displays no losses, with infinite voltage swing at precisely one frequency, as expressed by:

$$V_{out}(t) = V_o * cos[\omega_0(t) + \phi_0], \tag{2.1}$$

where the amplitude V_o, frequency ω_o, and phase reference ϕ_0, are all constants.

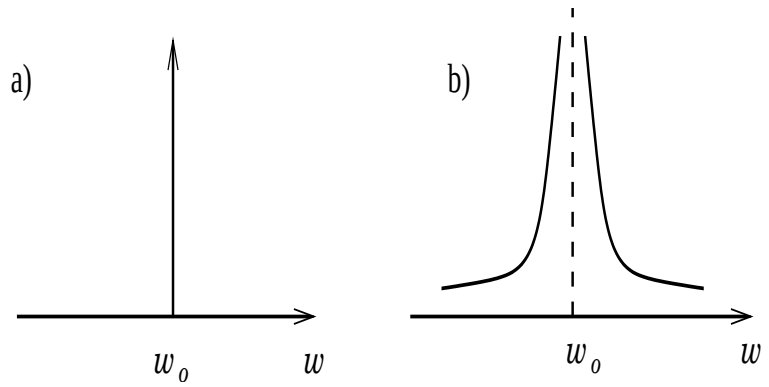

Figure 2.1: VCO frequency domain characteristics.

On the other hand, the real oscillator output is generally expressed by:

$$V_{out} = V_0(t) * f\left(\frac{\omega_{out}}{\phi(t)}\right), \tag{2.2}$$

where $V_0(t)$ and $\phi(t)$, are functions of time and f is a periodic function representing the steady state output of oscillation.

The oscillator performance is affected by the injection of different noise sources, such as thermal, shot and flicker noise by the devices that constitutes the oscillator itself, including active transistors and the passive elements.
These noise sources influence both the frequency or phase, and the amplitude of the output waveform.
Amplitude noise is usually not important because non-linearity that limit the

amplitude of oscillation also stabilize the amplitude noise [4]. The out-of-band (i.e. frequency offset) will tend to be rejected, as the oscillator is a frequency selective, or narrow band and high Q-factor circuit.
As a consequence of random fluctuations represented by $V_0(t)$ and $\phi(t)$, the spectrum $f(t)$ will have sidebands close to the oscillation frequency, Figure 2.1b.

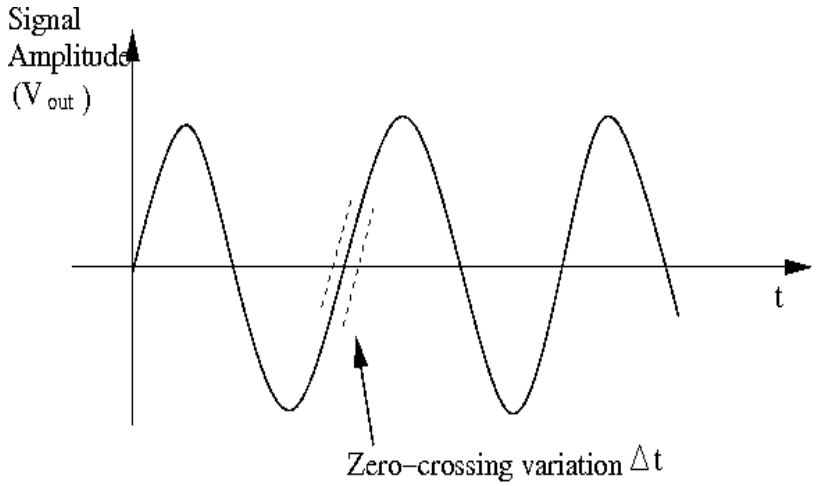

Figure 2.2: VCO time domain jitter.

The time domain behaviour of the oscillator resulting from the frequency fluctation is shown in Figure 2.2.
Fluctation in the time domain, known as jitter, is seen by the fact that the output voltage is not a pure sinusoid, as it displays a random perturbation of the zero-crossing of a periodic signal.
This behaviour result in a reduction of the fine tuning capabilities of the oscillator, that is needed to maintain a high quality for the data being represented to an FDSM application.

2.1 Oscillation criteria

One way to represent the LC-tank VCO is as two connected one-port circuits, as seen in Figure 2.3. In this model, one 1-port represents the frequency selective tank, where the oscillation occur, while the other 1-port represents the active, compensating elements, that cancel the losses in the tank.

In order to generate a periodic output, the oscillator circuit must entail a self-sustaining mechanism. This happens when:

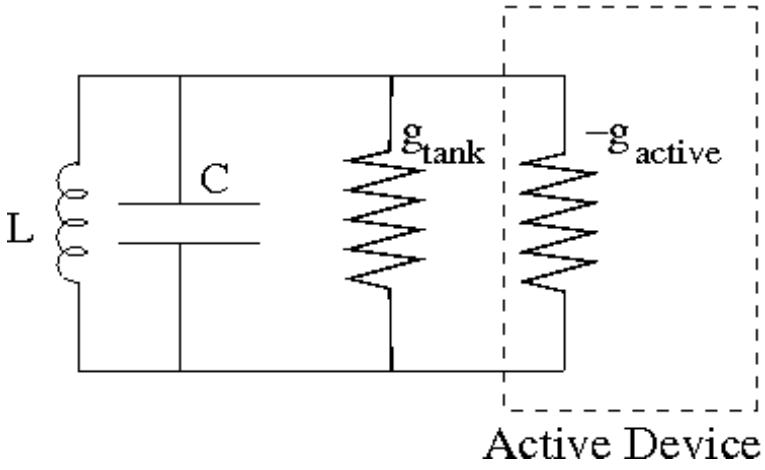

Figure 2.3: Steady state parallel LC-tank VCO model.

1. The negative conductance $(-g_{active})$ of the active elements compensates the losses in the tank (g_{tank}).

2. The closed loop gain has zero phase shift

In other words, the active elements act as a mean to transfer energy from dc power to the resonant tank, and if there is gain greater than or equal to unity magnitude, the oscillation amplitude will be large enough to fully commutate the oscillator bias current through the active elements, resulting in a square current wave that sustains oscillation.
During the energy transfer process, the active device also injects noise in the tank, dominating the phase noise contribution of the VCO.

The transfer of energy between the capacitor and the inductor can be explained from when the capacitor is fully charged by V_{dd}, then the capacitor will start to discharge through the inductor.
As it does, the inductor will create a magnetic field, and when the capacitor discharges, the inductor will try to keep the current in the circuit moving, slowing down the capacitor discharging, and charging up the other plate of the capacitor. Once the inductor's field collapses, the capacitor has been recharged, but with the opposite polarity, so it discharges again through the inductor. This oscillation will continue until the circuit runs out of energy due to tank losses.

The losses in the LC-tank are presented by three resistances: the series resistance of the inductor R_s, the series resistance of the capacitor R_c, and equivalent parallel resistance R_p.
R_p is not a straight forward design parameter, as it is given by:

$$R_p = \frac{L}{C * R_s}, \tag{2.3}$$

The quality factor Q, is a measure of how well the energy is conserved in the energy transmission between the inductor and the capacitor in the LC-tank [5]. The relation between the Q-factor and the equivalent parallel resistance is given by:

$$R_p = Q_{tank}^2 R_s \tag{2.4}$$

showing dependence on different properties of the VCO, such as the substrate parasites of both the inductor and the capacitor, and the loading effects of the active circuitry.
Parasitic resistance increase the losses, leading to higher g_{active} required from the active elements.

Generally, the inductor is the main source of Q-factor degeneration. This can be seen from the fact that even the parasitic capacitance have extremely high Q-factor, so the relevant Q-factor of the total capacitance is even higher than the varactor alone, thus underlining the limiting effect of the inductors-Q [6].

2.1.1 Barkhausen model

The Barkhausen 2-port model, seen in Figure 2.4, treats the LC-tank VCO as an active element G, and a feedback network H, and it will be analysed in order to reach what is know as the Barkhausen oscillator criteria.
The transfer function of the oscillator active elements $G(V, j\omega)$, and feedback network $H(V, j\omega)$ can exclude the dependence of the input amplitude (V) when assuming a linear amplifier and a linear feedback network, and may be expressed as functions of the angular frequency only.
Then the oscillator output voltage is expressed as:

$V_{out} = G(j\omega)V_G$,

and $V_H = H(j\omega)V_{out}$.

With

$V_G = V_{in} + V_H$

the transfer function of the complete network is calculated as:

$$\frac{V_{out}}{V_{in}} = \frac{G(j\omega)}{1 - H(j\omega)G(j\omega)}, \tag{2.5}$$

which is instable if $|H(j\omega)||G(j\omega)| \geq 1$.

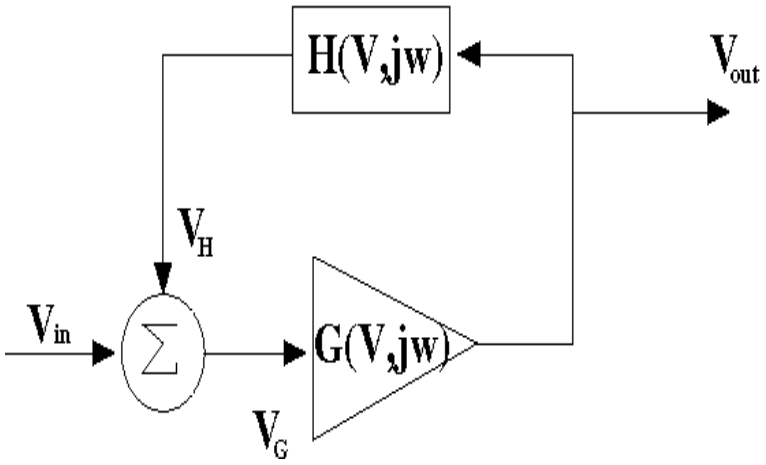

Figure 2.4: LC-tank VCO positive feedback system with frequency-selective network.

Typically, the magnitude of an initial loop gain is designed to be greater than one to guarantee oscillation. Then as the magnitude of the periodic signal increases, the magnitude of the loop gain is reduced to one by non-linearity in the amplifier in its steady state operation:

$$|H(j\omega)||G(j\omega)| = 1. \tag{2.6}$$

For the phase

$$\Phi_{G(j\omega)} + \Phi_{H(j\omega)} = 0 + 2\pi k, k = 1....n \tag{2.7}$$

is valid with $\Phi_{G(j\omega)}$ and $\Phi_{H(j\omega)}$, the respective phase of $G(j\omega)$ and $H(j\omega)$.

Assuming a zero degree phase shift over the active part $G(j\omega)$ there are no imaginary components, and $\Phi_{H(j\omega)} = 0$.
When the above mentioned conditions are satisfied, the circuit becomes lossless and oscillation occur.

2.2 Topologies

The LC-tank VCO topologies ranges from single transistor configurations that display less noise and increased robustness [6] , to more sophisticated ones, such as the noise shifting Colpitts oscillator, that takes into consideration the timing of the voltage and current waveforms in order to improve energy transfer efficiency, and thus reducing phase noise [7].
The basic LC-tank VCO configurations are often the same, with the compensating elements and the resonance tank, but with modifications for specific ap-

plications. If enough care is taken in the implementation, either one of the topologies can be fine tuned to work properly in an FDSM application.
In this section, two common LC-tank VCO topologies are shown.

2.2.1 Single cross coupled

The single cross-coupled LC VCO, seen in Figure 2.5a, has the input of each transistor in the differential pair connected to the output of the opposite transistor, resulting in the negative resistance.
This topology is widely used in high-frequency integrated circuits, due to the relative good phase noise, ease of implementation, relaxed start up conditions and differential operation.
The differential structure rejects undesirable common mode effects such as substrate and supply noise amplification and up conversion. This is important for a Si-based single chip to work properly, since the Si substrate is so conductive that noise from other circuitry is flowing through the substrate [8].

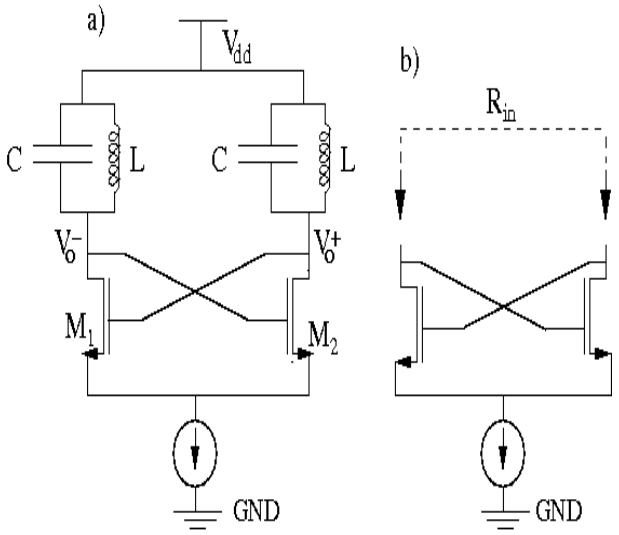

Figure 2.5: LC-tank VCO single cross coupled topology

For the oscillator shown in Figure 2.5, the bias current is coupled at the source terminal, however the bias can be coupled at the drain terminal, reducing sensitivity to variations in the supply voltage.
The single cross coupled differential topology may also be implemented using a cross-coupled pMOS pair [9], since the pMOS transistor itself claims lower noise characteristics, than the nMOS. On the other hand, the pMOS cross-coupled pairs can only provide negative resistance at lower frequencies, at higher frequencies, it behaves more like a power sinking load rather than a

power generating negative resistor, and there are other drawbacks as well [10]. Considering the cross-coupled feedback oscillator as a one port implementation, the negative resistance is seen at the drains of M1 and M2, and it is expressed as $R_{in} = -\frac{2}{G_{tank}}$ in Figure 2.5b.
As previously described, the negative resistance must overcome all real resistive losses in the oscillator circuit in order to make the circuit oscillates.

The tank voltage V_{tank} is the single-ended peak-to-peak voltage swing at either the $+$ or $-$ output node of the VCO, and it is given by

$$V_{tank} \approx \frac{2}{\pi} * I_{bias} * R_p. \tag{2.8}$$

From this equation, the relation between the tank amplitude and the losses in the tank is displayed.

2.2.2 Complementary cross coupled

Instead of a single transistor pair, a complementary nMOS and pMOS pair, seen in Figure 2.6, can be used to provide more positive gain [11]. The power

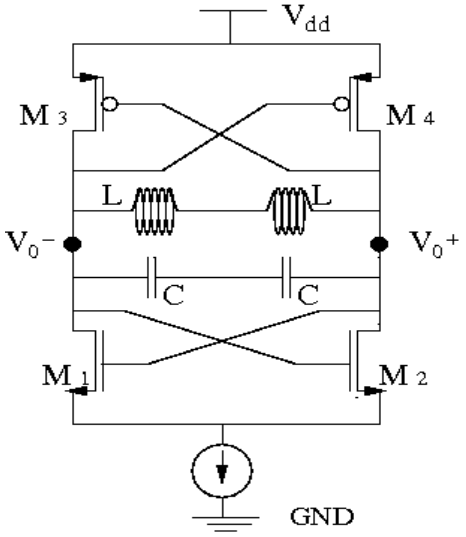

Figure 2.6: LC-tank VCO complementary cross coupled topology.

efficiency increase can be attributed to the increased current that flows through both the pMOS and nMOS devices, making the negative resistance twice as large, relaxing the start-up criteria.
Also, the double cross-coupled pair isolates the large oscillation signals $Vo+$ and $Vo-$ from V_{dd} and GND, reducing the coupling of the signal to the power supplies.

The total negative resistance provided by the nMOS and pMOS pair is given by:

$R_{negative,total} = R_{inn}//R_{inp} = -\frac{2}{g_{m12}+g_{m34}}$.

At high frequency of operation, an expression for the tank amplitude V_{tank} can be obtained assuming that the current in the differential stage switches quickly from one side to the other [11]. Due to finite switching time and limited gain the current waveform may be approximated by a sinusoid, resulting in a tank amplitude expressed as

$$V_{tank} \approx I_{bias} * Rp. \tag{2.9}$$

The importance of increased Q-factor of the LC-tank, is apparent as it translates to a larger effective tank parallel resistance R_p, this allows a lower oscillator bias current, while maintaining a large voltage swing, without clipping the signal amplitude at V_{dd}.
Operating with less bias current while maintaining the same amplitude, will result in improved phase noise performance. However, care needs to be taken for the complementary coupled LC-tank VCO, since the pMOS pair increasingly consumes voltage head room, so even if the nMOS pairs power consumption is reused, the total power is not necessarily reduced. In addition, adding a pMOS pair will introduce extra flicker noise, therefore the improvement in the phase noise may be negligible [10].

2.3 Operation trade offs

There are several parameters that determine the performance of an VCO, such as oscillation frequency, frequency tuning range, phase noise, and the power consumption. The interdependence of the design variables in the VCO, such as the inductor parameter, the total tank capacitance, the width and length of the transistors and the bias current is complex, resulting in a large number of approaches to improve performance. Specially, the inductor design has received a lot of attention , due to its important limitation on the Q-factor [12].
The LC-tank VCOs frequency tuning characteristics are closer examined in the next chapters.

This section briefly explains a design trade off that exist between the power consumption and phase noise [13][5] [12]. As can be seen from Leesons model [14], an semi-empirical phase noise model, the phase noise performance is better when the oscillator signal swing is maximized:

$$L(\Delta\omega) \propto \frac{N}{P_s Q_L}\left(\frac{\omega_c}{\Delta\omega}\right)^2, \tag{2.10}$$

where N is the noise factor, P_s is the signal power at the resonator, Q_L is the quality factor of the resonator with all the loading in place, ω_c is the oscillating

frequency and $\Delta\omega$ is an offset frequency from the carrier.

As the oscillator output frequency is affected by amplitude variations, it is dependent on the bias current when the oscillator is operating in the current limited region [15]. In the current-limited region, the oscillator tank amplitude V_{tank} linearly grows with the bias current according to Equation (2.8), until the oscillator enters the voltage limited region [13].

In the voltage-limited region, the supply voltage and also changes in the operation modes of the active elements (e.g., MOS transistors entering triode region), set an upper limit for the growth of the tank amplitude. When this limit is reached, the tank amplitude no longer grows with the bias current, therefore, further increase in the bias current will result in a waste of power. V_{tank} according to these two regions of operation, is expressed as:

$$V_{tank} = \begin{cases} \frac{I_{bias}}{g_{tank}} & (I - limited) \\ V_{limit} & (V - limited). \end{cases}$$

The best trade-off between power and phase noise, is often considered to be at the border between the current- and voltage- limited regions for typical LC-VCOs.

There is another phase noise trade-off that should be considered. When the amplitude swing of an VCO is increased, the SNR ratio will increase, and the thermal noise sources will have less impact on the Q-factor. However, with larger amplitude swings, there is the chance that the variable capacitance lying across it might become more unevenly distributed. This results in increased amplitude to frequency modulation (AM-FM) [16], which also contributes sidebands to the resonance frequency, which essentially is phase noise. The AM-FM modulation is further discussed in the next chapter.

2.4 Measurements

Depending on the intended applications of the VCO, different measurements are used under varying conditions to improve on the LC-tank VCOs performance. Descriptions of the different measurements can be obtained from designer application notes [4]. Typical measurements include frequency pushing, that describes variation in the oscillator output frequency due to change in the power supply. Already mentioned is the importance of the phase noise in the oscillator, and it has attracted a lot of attention, as it is a major VCO performance limiting factor.
The output frequency vs. tuning voltage is a fundamental parameter, leading to the tuning sensitivity (Hz/V), which is the differential of the output frequency versus tuning voltage curve. This parameter is important when measuring the

frequency output of the LC-tank VCO, in order to see if it resembles that given by Equation (1.1). Also, the resolution of the FDSM system will depend on the tuning voltage sensitivity.
The power dissipation is another factor, which arises from dynamic power dissipation, such as the switching current from charging and discharging parasitic capacitances, and also static power dissipations.
VCOs typically suffer from the trade-offs between speed, power dissipation, and noise.

2.5 Summary

For the purpose of this thesis, where the main focus is on the varactor, it is necessary to get an understanding of the mechanisms behind the frequency generating LC-tank VCO and its operation. This chapter was intended as an introduction to these basic mechanisms, without going to deep into the detail, only just enough to know what to expect. This way, the functionality of the varactor is put in a context, making it easier to see the bigger picture.
When configuring a LC-tank VCO, there are several choices and trade offs to be considered in order to get the desired functionality. However, most LC-tank VCOs are based on the same basic configuration, and can be optimized for specific application, if enough time is invested.
The LC-tank VCO that eventually was designed for this thesis, is the single-cross coupled one, and a reasoning for this choice is given in the **Design and analysis** chapter.

3 Variable MOS-capacitors

As an introduction to this chapter, an explanation is given as to what a capacitor really is:
The capacitor is a device that stores energy in the electric field created between a pair of conductors on which equal but opposite electrical charges have been placed.
Its capacitance is defined as the charge $q(v)$ with respect to voltage,

$$C(v) = \frac{dq(v)}{dv}, \tag{3.1}$$

while the current through a capacitor is simply the time-derivative of the charge

$$i(t) = \frac{dq(v(t))}{dt}. \tag{3.2}$$

In other word, the capacitor works almost like a battery that may be charged, or discharged.

3.1 Tuning devices

Varactors are sources of variable capacitances, and are used as frequency tuning elements in the LC-tank VCOs.
One option when tuning the LC-tank VCOs, is to use a reverse biased p-n junction varactor. However, this varactor does not scale with technology, and suffers from low C_{max}/C_{min}, limiting the available frequency tuning range. In addition, there is the possibility that the p-n junction varactor may become forward biased with large-amplitude swings, leading to additional losses in the circuits.
Another well known varactor readily available in CMOS technology, is the MOS transistor itself. An nMOS varactor is illustrated in Figure 3.1 consisting of a thin oxide layer, a top metal contact representing the poly gate, and a p-doped substrate. A second metal layer forms an Ohmic contact to the bulk of the semiconductor.
The capacitance vs. area ratio is higher for the MOS-type varactor than the p-n junction varactor, resulting in higher capacitance tuning ranges [16].
The MOS-varactors are also showing strong capacitance variation within a few hundreds of milli-volts, making them useful for low power operating circuits.
As MOS-varactors scale with the developing technology, their performance is

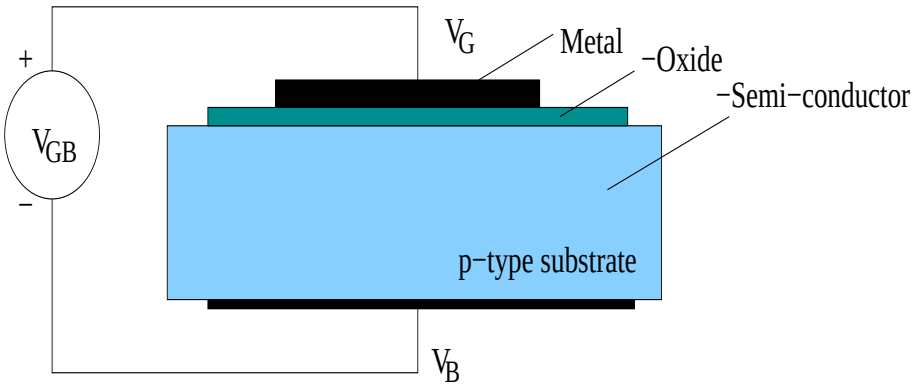

Figure 3.1: Illustration of an n-type MOS-varactor structure.

improving with every new process step. The increasing doping levels of the transistors are reducing the resistive losses, and resulting in VCOs with lower power consumption and lower phase noise.
Different MOS-varactor configurations have been tested in order to achieve high Q-factor and wide tuning ranges [17].

3.2 Capacitance regions

The small-signal capacitance characteristics of an MOS varactor, with the source and the drain tied to the bulk, is displayed in Figure 3.2.
This varactor has a capacitance curve that varies non monotonically with the bias voltage, since it operates in the inversion, depletion and accumulation regions [18]. The bias voltage V_{GB}, represents the applied gate and bulk terminal voltages. The gate-oxide capacitance in the accumulation and inversion regions, is represented by:

$$C_{inv,acc} = C_{ox} = \frac{\epsilon * W * L}{t_{ox}} = C_{max}, \tag{3.3}$$

where $W * L =$ represents the area of varactor, t_{ox} is the oxide thickness, ϵ is the permittivity of silicone dioxide.
The depletion region capacitance consists of an series connection to the C_{OX}, and is represented by :

$$C_{dep,tot} = \frac{C_{ox} * C_{dep}}{C_{ox} + C_{dep}} \approx C_{min} \tag{3.4}$$

For large signal amplitude swing at the D=S=B varactors gate, the resulting effect on the capacitance is also displayed in Figure 3.2.
The instantaneous value of the capacitance is changed throughout the signal

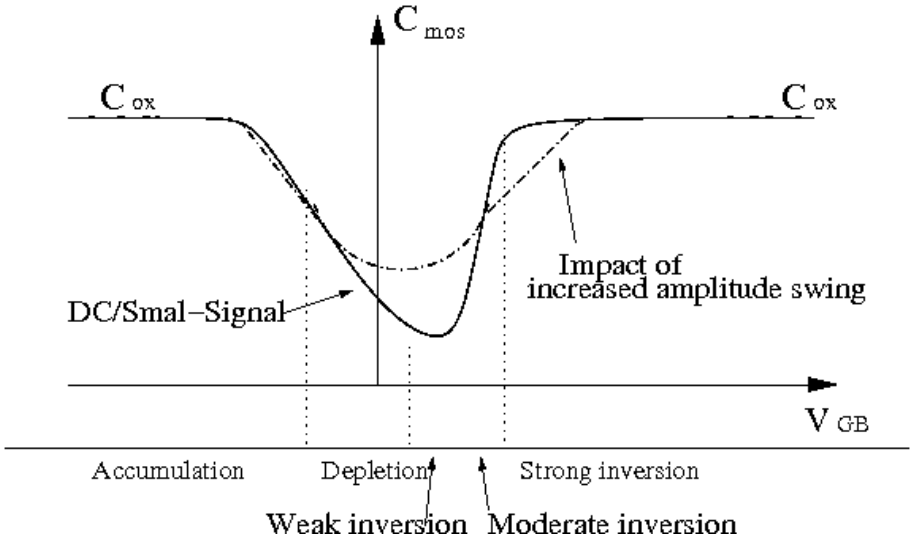

Figure 3.2: The D=S=B varactors tuning characteristics.

period, and the effective tuning range of the VCO is significantly reduced, as the capacitance floor is raised. The average value of the capacitance over a single output frequency period is still a function of the varactor bias level V_{GB}, but the tuning ability of the circuit is impaired by the non monontonicity of the variable capacitance.

Figure 3.3 illustrates the relation between the channel charges in an MOS-varactor, under different biasing conditions [14].
The voltage that is found between the accumulation and depletion regions is referred to as the flatband voltage, V_{FB}.
If the threshold voltage V_T of the transistor is exceeded by a voltage applied at the bulk V_B that is much greater than the gate voltage V_G, an accumulation channel with mobile holes builds up and forms a parallel plate capacitor with the poly gate.
On the other hand, for a positive voltage V_G exceeding V_T, and being much greater than V_B, an inversion channel will form, allowing negative charged carriers to move freely. Then the MOS-varactor is working in inversion mode, acting as a gate-oxide capacitor with the opposite polarity of the transistor working in accumulation mode.
For intermediate values of V_{GB}, where the varactor bias level is between V_T and V_{FB}, few mobile charge carriers are to be found at the gate oxide interface. As a result, the available capacitance is decreased, and the varactor will be working in the depletion mode.

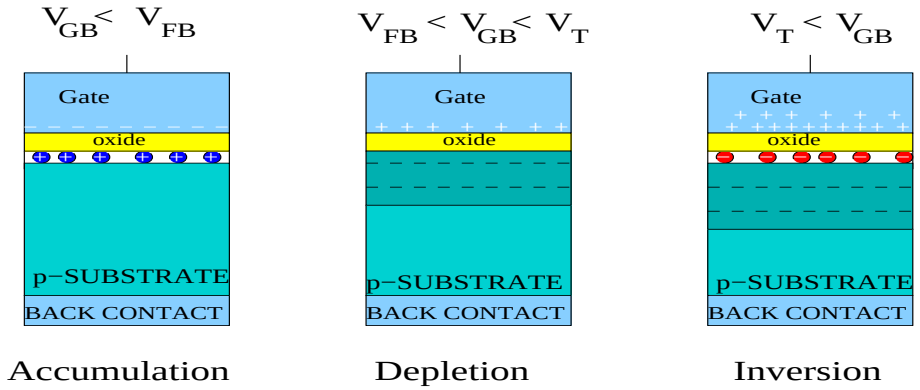

Figure 3.3: Illustration of gate- and channel charges of the MOS-varactor operating in accumulation, depletion and inversion modes.

3.2.1 Inversion mode varactor

Varactors with steep capacitance characteristics are favourable in low power operating VCOs, when wide tuning ranges are required.
If the bulk of the D=S=B varactor is decoupled and tied to the voltage supply V_{dd}, as shown in Figure 3.4a, the varactor does not enter the accumulation region for a very wide range of gate voltage V_G values.
This device, called the inversion mode varactor, displays an almost monotonic capacitance function, and has a wider tuning range than the D=S=B varactor, Figure 3.4b.
The monotonicity of the dc/small-signal curve prevents the tuning range degradation by the amplitude swing, which was seen in the case of the D=S=B varactor. Another benefit from using an IMOS-varactor is that its n-well connection is tied to V_{dd} rather than a tuning voltage, and therefore the device is less vulnerable to latch-up[1].

3.2.2 Accumulation mode varactor

Another MOS varactor not suffering from the limitations of the D=S=B varactor, is one that operates in the depletion and accumulation regions only, shown in Figure 3.5a. This device is not surprisingly called the accumulation- mode varactor, and it also displays abrupt, nonlinear, monotonic capacitance characteristics, seen in Figure 3.5b.
The AMOS is derived from a pMOS transistor, in which the p+ source/ drain regions are replaced by n+ well contacts, making sure the formation of the strong, moderate, and weak inversion region is inhibited, due to suppression

[1] A condition that can occur in CMOS circuits where parasitic nMOS and pMOS transistors are both conducting and remain conduction once the disturbance that started the conduction is removed

of holes injected into the MOS channel [19].
This varactor configuration also takes away the need for a negative supply voltage. The AMOS-varactor has shown, less parasitic resistance and lower phase noise at large offset frequency from the carrier, when compared to the IMOS and the junction varactors [19].
The C_{max}/C_{min} capacitance ratio for the AMOS is about the same as for the IMOS-varactor, usually around two, but it can grow even larger with increased tuning voltages.
This rather low value is caused by the presence of the overlap capacitance between gate and drain/source, that makes up for more than half the value of C_{min} [14].
Unfortunately, the n+ source/drain in an n-well varactor was not available for this thesis.

3.3 Capacitance tuning characteristics

The frequency tuning curve of the LC-tank VCO is not easy to predict, as it substantially deviates from the ideal curve in Equation (1.1), when using a steep varactor and the full oscillator amplitude swing is applied directly across it. The instantaneous value of the capacitance will change throughout the signal period, and it shows strong dependence on the amplitude, which is set by the bias current in the current limited region (Section 2.3).
Even if the bias current was omitted [15] , there are still other sources of am-

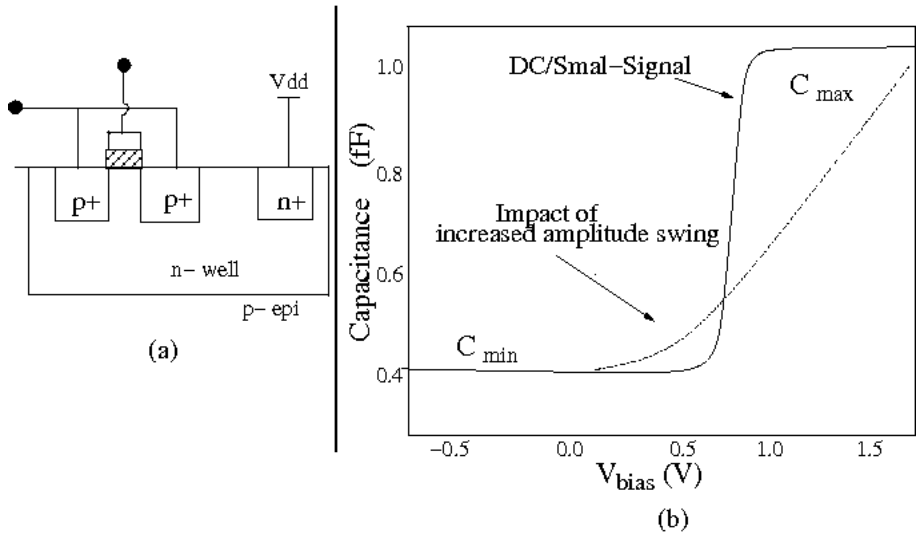

Figure 3.4: Illustration of the IMOS-varactor and its capacitance tuning characteristics.

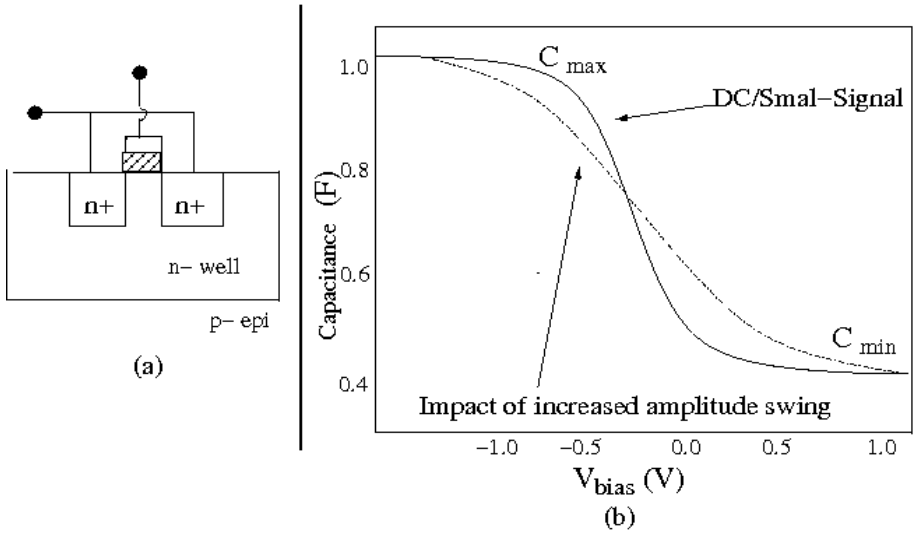

Figure 3.5: Illustration of the AMOS-varactor and its capacitance tuning characteristics.

plitude variations. Variations in the power supply voltage and substrate noise [8], are two such sources, however their impacts are not closer examined in this work.

3.3.1 Swing average capacitance

When evaluating the LC-tank VCOs frequency tuning curve, it is important to take into account the fact that the full oscillation swing is applied across the varactor.
Swing average capacitance ratios [16][18], mimic the large signal situation in the VCO, thus it provides a more realistic frequency tuning curve based on the capacitance and tuning voltage relation, than small-signal capacitance curves.

The swing average capacitances can be approximated with:

$$C_{av}(V_{tune}) = \frac{1}{V_{DD}} \int C(V_G, V_{tune}) \Delta V_G, \tag{3.5}$$

with the integral taken from minimum to maximum tuning voltage, while V_G represent the oscillation swing at the varactor gate.

The average tuning range is set by the swing average capacitance.

$$C_{av,ratio} = \frac{C_{av,max}}{C_{av,min}} \tag{3.6}$$

The impact of variation in capacitance due to varactor bias level V_{bias}, and amplitude swing on the output frequency, can be seen from Figure 3.6.

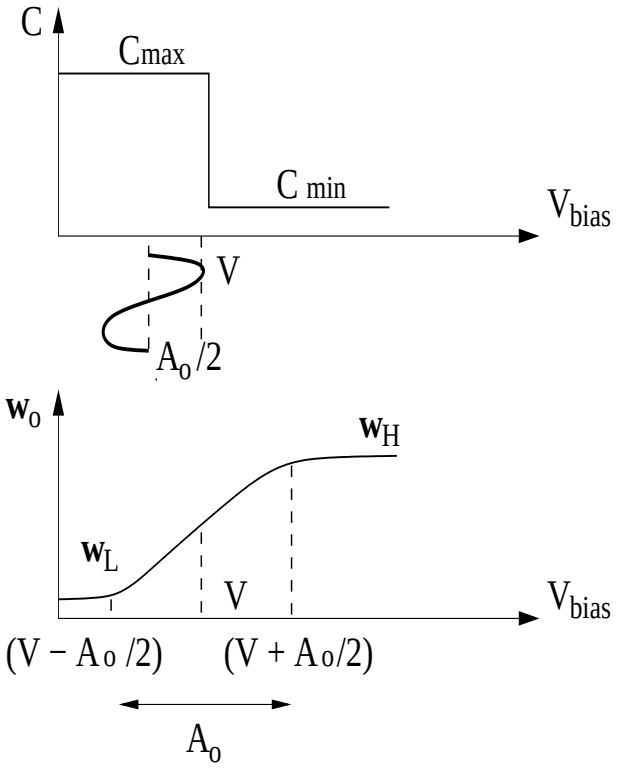

Figure 3.6: Illustration of the small-signal characteristics, and the impact of the VCOs amplitude on the frequency tuning curve.

The varactor capacitance is shown to have zero rise and fall time at V, which is an exaggeration, while the oscillation amplitude A_0, is assumed constant over the whole voltage tuning range.

For low tuning voltages (V - $\frac{A_0}{2}$), the tank capacitance equals C_{max} over the entire oscillator swing and display a flat characteristic. The output frequency is given by:
$\omega_L = \frac{1}{\sqrt{LC_{max}}}$.

At high tuning voltages (V + $\frac{A_0}{2}$) the varactor stays in the depletion region for a wide range of gate voltages, showing little capacitance variation and flat characteristics, with output frequency:
$\omega_H = \frac{1}{\sqrt{LC_{min}}}$
At medium tuning voltages V, the transition from C_{max} to C_{min} occurs during the signal swings, resulting in high capacitance variation. In this region the out-

put frequency is interpolated between two limit values ω_L and ω_H. When the tuning voltage drives the variable capacitor towards the C_{max} region, the capacitance value across the amplitude swing increases and the period of oscillation slows down. When the varactor is pushed in the direction of the C_{min} region, the capacitance values across the amplitude lowers and the period shortens.

The effective capacitance tuning range is lower than the absolute tuning range, due to the smoothing effect on the output frequency. This results in reduced VCO gain, which in the centre of the tuning curve, can be expressed as:

$$K_{VCO} = \frac{\omega_H - \omega_L}{A_0}, \tag{3.7}$$

where A_0 is assumed to be constant.

Generally, the VCO gain is expressed with the frequency variations as a function of tuning voltage variation [2]. Ideally the tuning sensitivity would be constant, but this is generally not the case, particularly not for an abrupt varactor. Often low tuning gain, MHz/V_{tune}, is desired since it generally produces lower phase noise due to the varactor being loosely coupled at the tank of the oscillator [3].

3.3.2 Zero AM-FM modulation

One interesting feature of the amplitude impact on the varactor capacitance is shown in Figure 3.7. This figure is a simplification, since in reality the capacitance is changing slowly at the maximum and minimum capacitance, while the transition between the two is smoother.
As seen, there is approximately zero AM - FM modulation at $V_{bias} = V_{middle}$, and also when the amplitude swing is lying entirely in the flat capacitance regions. In the later case, the amplitude never crosses the steep capacitance step, and therefore the capacitance is evenly distributed across the VCOs amplitude swings. At $V_{bias} = V_{middle}$, a time-average capacitance is lying across the amplitude swings, since the signal stays for one half of its cycle in C_{max} and the other half at C_{min}.
AM noise is generally far enough below FM noise in an oscillator that it is of little concern. However, FM noise can be more significant and should not be taken for granted since it can be the limiting factor in applications like narrow band communications links, frequency synthesizers, Doppler radars, etc. It limits the range resolution, sensitivity, and channel spacing of these systems [4].
Earlier it was mentioned that the $\Delta - \Sigma$ converters outperform the more traditional Nyquist rate converters in situations where high resolution and low

[2] $http://www.silabs.com/public/documents/tpub\_doc/anote/Timing/XO/VCXO/en/AN255.pdf$
[3] $http://www.maxim-ic.com/appnotes.cfm/appnote\_number/2041/$
[4] $http://www.emfsystems.com/100.htm$

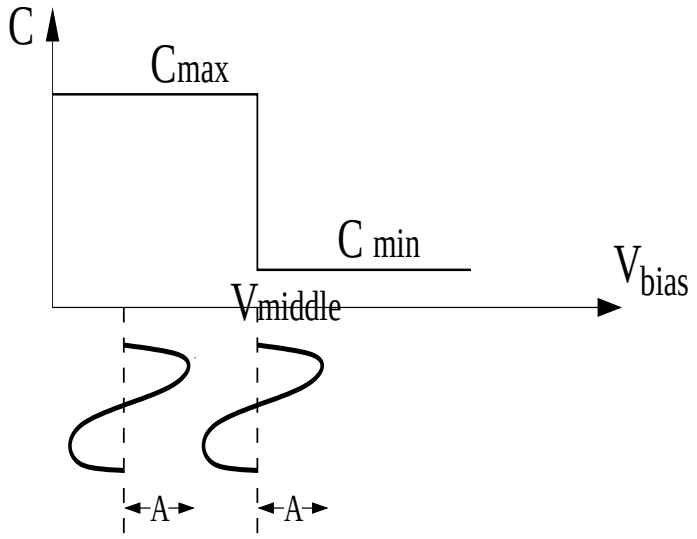

Figure 3.7: Illustration of zero AM-FM modulation regions.

signal bandwidths are needed. From this it becomes even more clear that the AM-FM modulation factor needs to be taken into consideration for the FDSM system.

Usually, the easiest way to achieve reduced steepness of the varactor capacitance curve, is by adding large parasitic capacitances. However, this approach has the disadvantage of extremely reduced tuning range.
Another way to influence varactor capacitance and therefore the frequency tuning of the VCO, is seen in the next section, where differential doping is used on multi-finger poly-gates.

3.4 Impact of differential gate doping

The capacitance curve of a steep multi-finger varactor can be influenced by specifying the doping profile of the poly-gate. This issue is discussed in [20], where the impact on frequency tuning, phase noise and also variations in frequency sensitivity due to V_{dd}, is presented.

There are three possibilities for the gate doping, either homogenous doping with negative or positive doping only, or a mixture, with the fingers having alternating n and p doping. The influence of different gate doping on a accumulation mode varactor is displayed in Figure 3.8, where differential np gate doping introduce a shift in the flatband voltage. For n-doped gates, the flat band voltage is low, close to 0 V, but it is shifted by approximately 1 V, when using p-doping on the multi-finger gate. For the varactor with mixed nega-

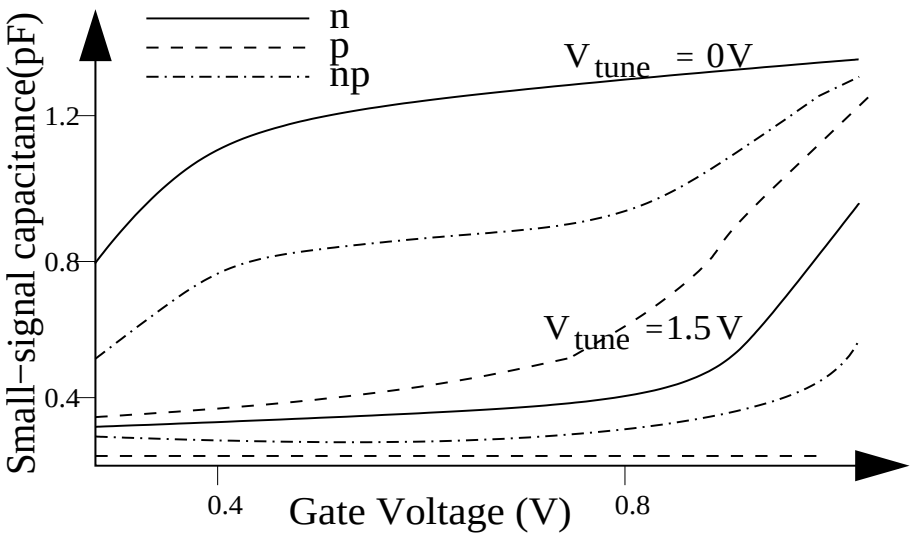

Figure 3.8: The effect of differential gate-doping on the capacitance lying across the VCO amplitude swing.

tive/positive gate doping, the capacitance is an average between those of the two varactors with entirely negative or positive gate doping.
The capacitance curve becomes less steep for the mixed doped gate, therefore the linearity is improved, as the varactor capacitance is more evenly distributed over the VCO signal swings. The differential doping also result in reduction in close-in phase noise, and reduced max sensitivity to variation in supply voltage.
The homogenous negative and positive doped gates increase the absolute VCO tuning range, but for the positive doped gate the average capacitance tuning range, becomes much smaller than the absolute tuning range, when compared to the negative doping and mixed doping of the gate. This is a factor resulting the swing averaging process, therefore positive gate doping is less viable for VCO implementation, although at low capacitance values it does display high Q-factor.

3.5 Other tuning methods

It is possible to decouple the tuning range from phase noise, at the price of somewhat more complicated control scheme.
An array of fixed capacitors[21][22], selected by a digital word can tune the oscillator to a set of discrete frequencies. It is sufficient that the varactors variable capacitance cover the largest gap between adjacent discrete frequencies, not the

full capacitance range. With more elements in the switch capacitor array this gap reduces to smaller fractions of the full tuning range. The main point is that fixed capacitors do not convert AM to FM, only the varactor does. In this way the tuning range may be expanded arbitrarily by adding more elements to the capacitor array without worsening the sensitivity to AM-FM conversion, or, for a given tuning range, the sensitivity may be lowered, increasing linearity. A number of capacitors are used, one for each tuning range. A series switch digitally selects which capacitor to use. The switch is usually a MOSFET transistor that is biased on or off. Its channel resistance is low so that the loss does not degrade the LC-tank VCOs Q-factor. The fine tuning of the capacitance is achieved by using a small-valued varactor.

3.6 Summary

This chapter deals with the important capacitance tuning characteristics of MOS-varactor structures, providing insight in order to understand their behaviour, and their frequency determining capabilities.
One impression this chapter leaves behind, is that there are limitations in the ways to improve on the MOS-varactors, in order to get the desired tuning characteristics. This issue is later addressed in the **Varactor combinations** chapter, while the next chapter provides some practical insight to the tuning issues.

4 Design and analysis of LC VCO using MOS-varactor

The schematic of the single cross coupled LC-tank VCO designed in STM90 90 nm CMOS technology, with a 0.9 V supply voltage, is shown in Figure 4.1.
The reasoning for using this topology is that it is well suited for applications operating at high, and still increasing frequencies, with steadily lower supply voltages [10].
The additional pMOS cross-coupled transistors used in the double cross-coupled topology, were omitted due to their contribution of parasitic capacitance, that result from its reduced transconductance. Also, more voltage headroom would have been consumed with the additional pMOS cross coupling [9].
Still, the negative conductance $-G_m$ provided by the nMOS active elements, is required to be large enough to compensate the losses in the LC-tank. Therefore the length of the active compensating transistors was set at 0.2 μm, while the width was set at 2.5 μm, as a compromise between the VCOs phase noise, parasitic capacitance and the available capacitance tuning range.

The $C4$ capacitor seen in parallel with the bias current in Figure 4.1 provides some attenuation of high-frequency noise components coming from the bias current.
Also, the bias current source is often considered the most significant contributor of flicker noise in a cross coupled differential oscillator.
One way to deal with this problem, is to use a pMOS transistor as the bias current source, since it display lower flicker noise up-conversion than the same dimension nMOS transistor [6]. By keeping the w/l dimensions of the pMOS transistor high, the voltage drop on it will be lower, since it will be operating in saturation. This results in improved symmetry for the LC-tank VCO output waveform, that will reduce the up conversion of flicker noise.
The IMOS-varactor is seen implemented differentially, with two equally sized pMOS transistors(M6,M7) having their source and drain nodes tied with the tuning voltage V_{tune}, while their bulks are connected to V_{dd}.
The gate nodes of the differential varactor are connect in parallel with a differential inductor structure, to form the overall tank circuit structure.
Additional capacitances were placed over the LC-tank VCOs active elements, these do not add thermal noise, and they remove high frequency noise components.
Primarily, the length of the multi-finger MOS-varactor was set to the minimum

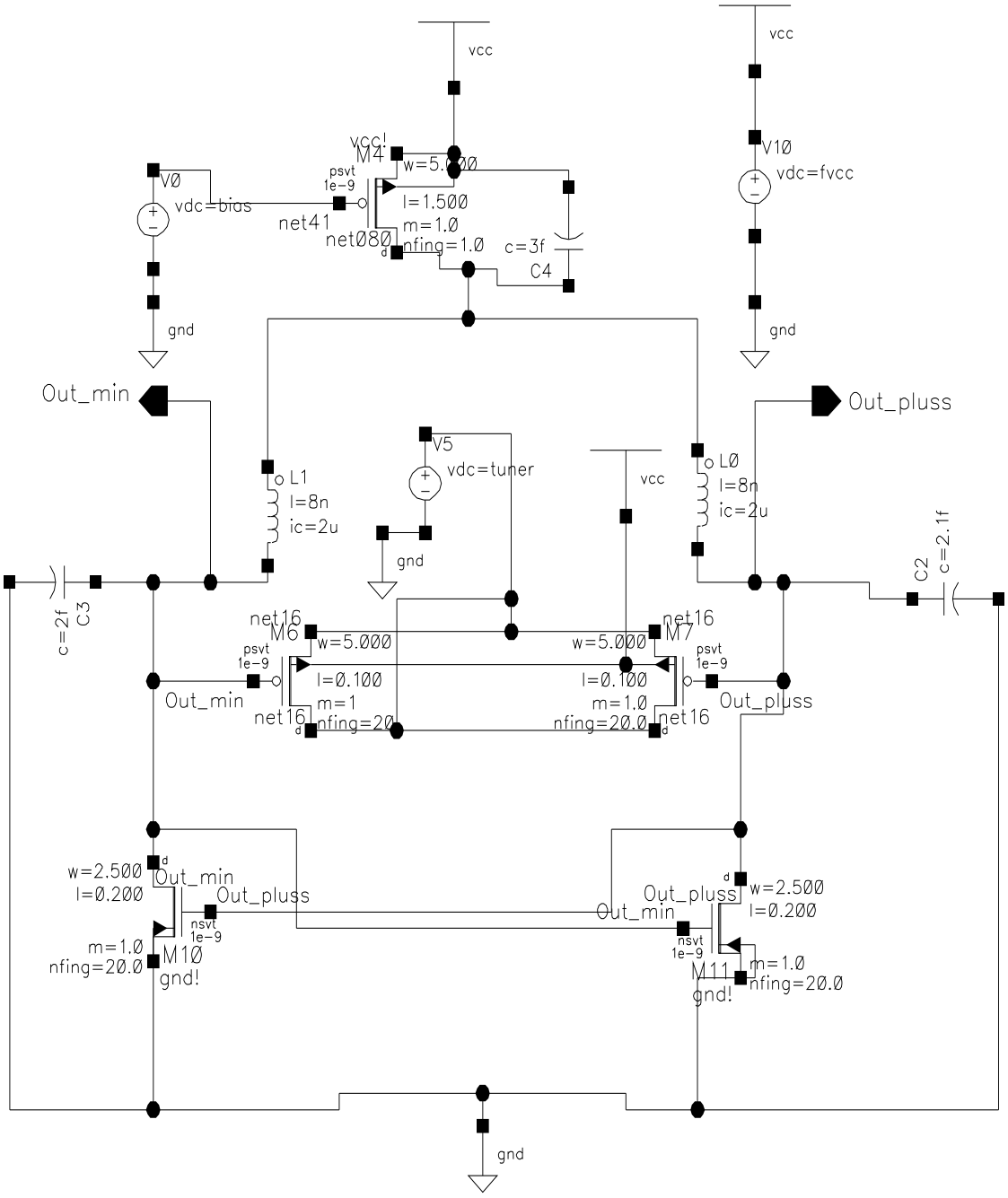

Figure 4.1: The LC VCO schematics.

size allowed, 0.1-um, this in order to keep the channel resistance low, and not

to degrade the Q-factor.
Varactors with finger widths of 1 - 5 μm display the highest FOM when finger lengths are < 0.5 μm according to [17]. The output frequency that results from using minimum transistor lengths, and a constant inductance value at 8 nH is quite high, as it approaches the 13 GHz frequency region. Obviously this frequency is way too high for the FDSM application to handle, therefore the frequency need shifted down to a more practical range. Usually, an prescaler will be used to carry out the division. The frequency division is further explained in the yet to be finished master thesis of Ehsan Arshad, where it is also shown that available frequency tuning range is significantly reduced by the division.

4.1 Varactor small-signal test circuits

MOS-varactor small-signal curves, not impaired by the LC-tank VCOs amplitude swings, are derived by using simple test circuit such as the one in Figure 4.2.
As seen, this is the IMOS-varactor structure, with the bulk connected to V_{dd}, while the tuning voltage is applied at the tied drain and source terminals. This test circuit represents variable capacitance on one side of the differential LC-tank VCO.

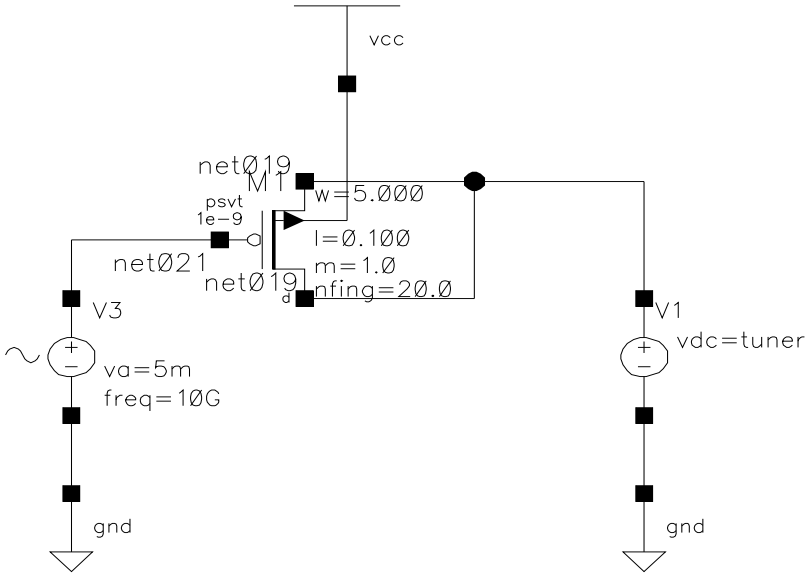

Figure 4.2: IMOS-varactor small-signal test circuit.

The procedure used in the Cadence environment to simulate and plot MOS-varactor capacitance curves, such as those seen in Figure 4.4, is the following:

1. In the analog environment, the operating point was saved in an DC-analysis.
2. Second, a parametric analysis was performed, where the tuning voltage was stepped across the varactor being analysed.
3. Then, from the calculator window the operation point (op) was selected, providing a list of parameters, including *cgg* which represents the gate-oxide capacitance of the varactor.
4. From there the capacitance curves were plotted from using the calculator plot button.

Like the IMOS test circuit, the D=S=B varactor was also set up as an test circuit, and their dimensions where kept the same, to get an comparison of their capacitance tuning characteristics.

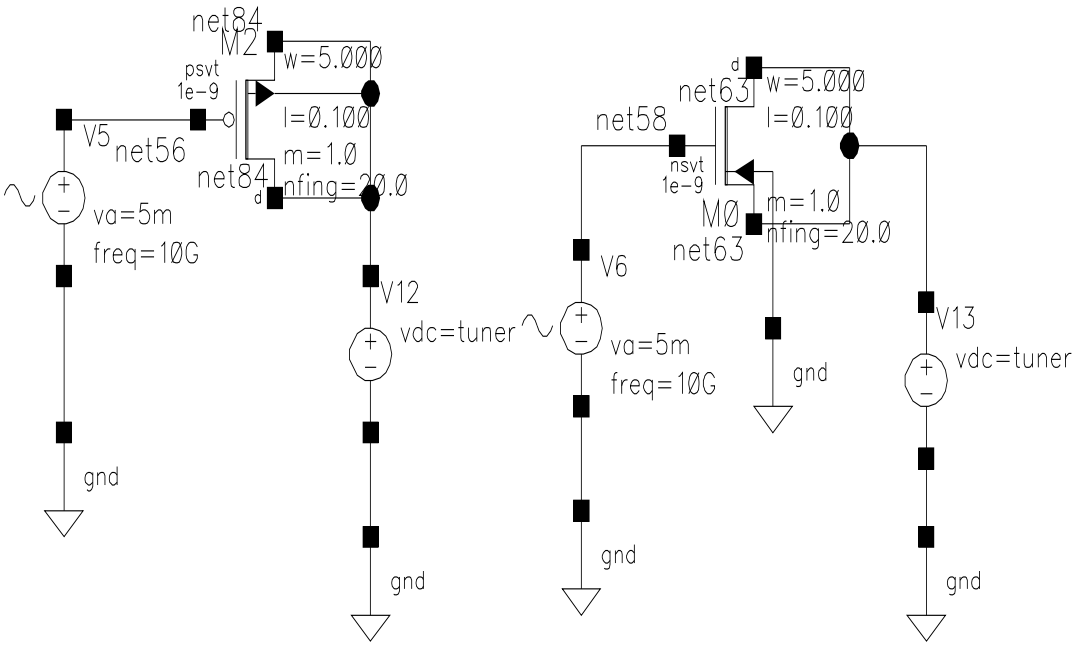

Figure 4.3: The D=S=B and NBG-varactor small-signal test circuits.

From Figure 4.4 it is seen that the D=S=B varactor operates in the accumulation, depletion and inversion regions.
For low power operation, the tuning voltage should obviously not exceed the supply voltage, but in order to demonstrate the capacitance characteristics, the

tuning voltage was tuned over a wide area, going from -1 to 1 V.
The D=S=B varactor displayed C_{min} = 4.29 fF around V_{tune} = -220 mV and C_{max} = 7.07 fF at V_{tune} = 1 V.
As expected from the varactor chapter, the IMOS-varactor display an larger, steeper, and more monotonic capacitance characteristic, than the D=S=B coupled varactor, giving it a larger frequency tuning range.

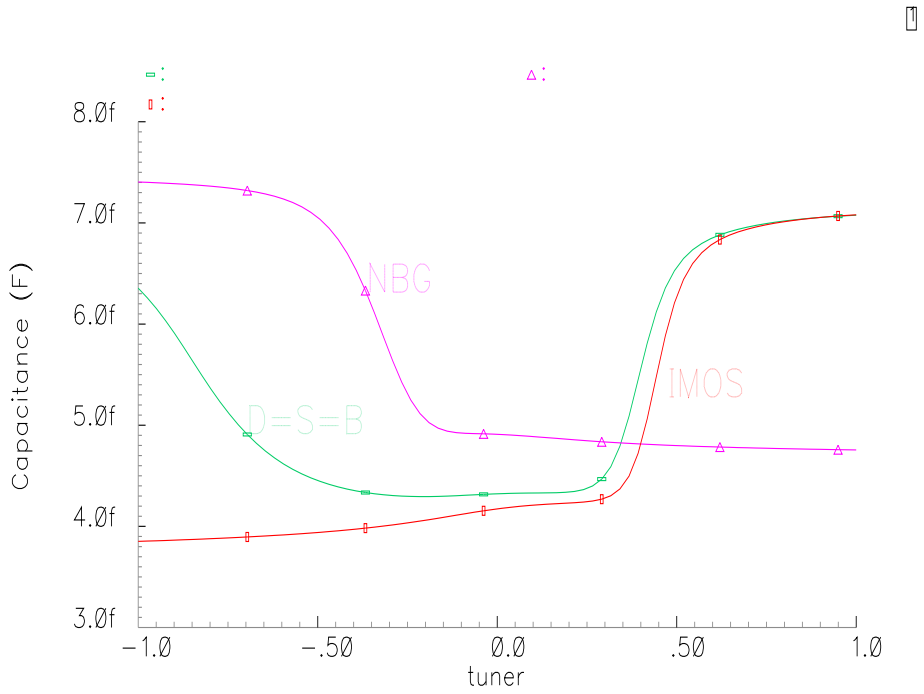

Figure 4.4: The IMOS, D=S=B and NBG varactor small-signal characteristics.

The characteristics of another MOS-varactor, with the bulk connected to ground and the drain/source terminals connected to the tuning voltage, is also shown in Figure 4.3. Since this MOS-varactor apparently has no name attached to it, for simplicity it will be called the NBG-varactor, indicating that its based on an nMOS where the bulk is connected to ground.
The NBG-varactor capacitance curve is plotted along with the IMOS and D=S=B capacitance curves in Figure 4.4, where its dimensions are kept the same as the other two varactors.
The NBG-varactor also displays an almost equally large tuning range as the IMOS configured varactor, with a monotonic and steep capacitance curve.

Compared to the IMOS, the NBG-varactor operates at slightly higher capacitance values, and therefore at slightly lower frequencies.

The maximum and minimum capacitance values where $C_{min} = 4.75$ fF at $V_{tune} = 1$ V and $C_{max} = 7.40$ fF at $V_{tune} = -1$ V.

4.2 Impact of amplitude swings

The influence of the bias current on the IMOS-varactor small-signal capacitance curve, is shown in Figure 4.5.
The common mode level of the LC-tank VCO is modulated by low frequency noise related to the bias current. This affects the amplitude, causing change in the varactor bias level, and ultimately to frequency variations [15].

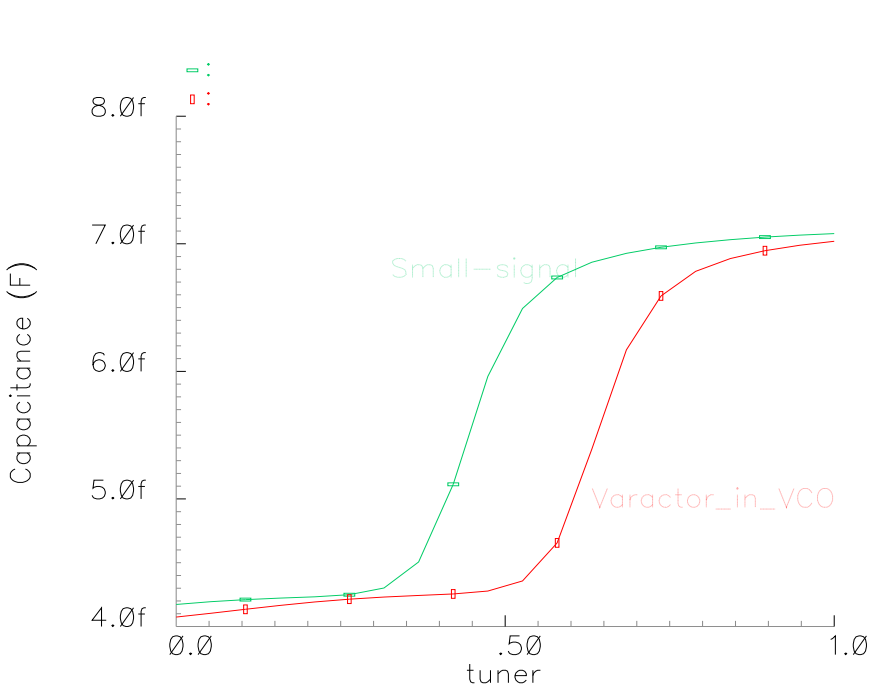

Figure 4.5: IMOS-varactor small-signal characteristics, and the impact of varactor bias distortion.

As a result of this modulation effect, the varactor small-signal curve is shifted to the right.
One way to reduce this unwanted amplitude modulating effect, can be to all-in-all eliminate the bias current from the LC-tank VCO design, since this will provide improvements in the close-in phase noise [15].
This possibility is not further explored in this work, since the bias current is actively used to set different amplitude values for the LC-tank VCO, in order to display the impact on the frequency output. However, one approach in order to reduce the common mode effect can be seen from [23].

The abrupt regions in varactors causes the most frequency distortion.
In slower varying and less abrupt regions, the capacitance will be more evenly distributed across the amplitude swings. The IMOS-varactor capacitance characteristics were displayed in Figure 4.4 across a wide tuning region. In Figure 4.6 the IMOS characteristics are plotted again, but this time only for the slower varying, and flat region, going from V_{tune} = -1 to 0 V. This region has a significant lower C_{max}/C_{min} relation, with C_{max} = 4.17 fF and C_{min} = 3.85 fF, resulting in a severely reduced frequency tuning range.

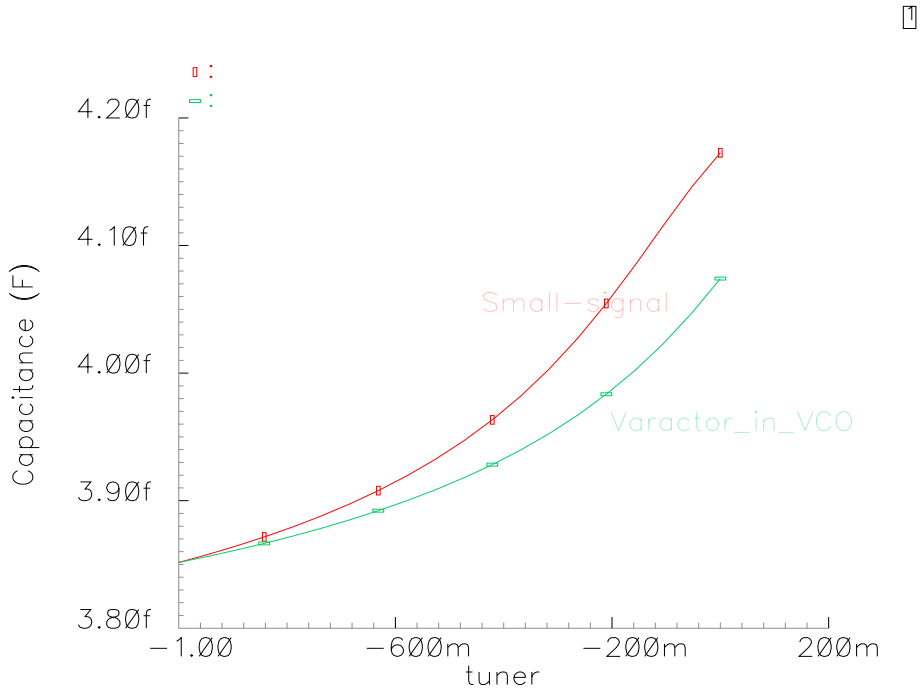

Figure 4.6: Comparison of the IMOS varactors small-signal and the actual VCO implemented capacitance, over an slow varying capacitance region.

Using the test circuit of the IMOS-varactor once again, the impact of the varying gate voltage on the small-signal characteristics was easily derived. This was done by stepping a dc voltage from -1 V to 1 V at the gate of the test circuit, and can be seen from Figure 4.7. In this simulation, the tuning voltage over the tied drain source was kept constant, first for the maximum tuning voltage 1 V, and then for the minimum value of 0 V.
In the LC-tank VCO designed, almost none negative amplitude values are found lying across the MOS-varactors. However, in Figure 4.7, this was done deliberately to show how the capacitance is varying with the gate voltages. It is seen that with large gate voltage swings, the instantaneous value of the

capacitance will change throughout the oscillation periods.

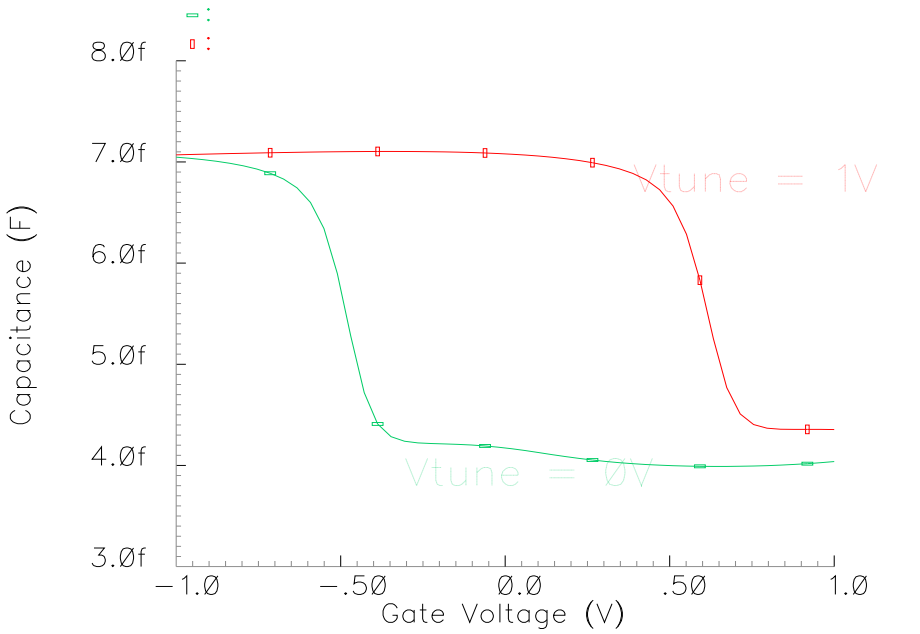

Figure 4.7: Varying capacitance across the VCOs large singal output swing.

4.2.1 The amplitude swings impact on the frequency output

To further elaborate on the impact of amplitude variations on the output frequency, simulation of the oscillator frequency as a function of the tuning voltage, was performed while setting different output amplitude values with the bias current.

The dc voltage supplied at the bias current transistor gate was set to 600 mV. The dimensions of pMOS transistor used to provide the bias current, was kept constant at $5\mu m$, while the length was adjusted to provide the desired amplitude values, shown in Table 4.1.
The amplitude value resulting from setting $L = 0.5\ \mu m$ was 526 mV with the bias current at 9.17 μA, and for $L = 1.5\ \mu m$ it was 428 mV, with the bias current value at 3.68 μA.
These values kept the oscillator well inside the current limited region, as the amplitude was still growing with the bias current for $L = 0.2\ \mu m$, where the amplitude value was 608 mV, while the bias current I_{ds} showed 16.58 μA.

No attempts were made to find the often preferred operation point where the best power and phase noise trade-off can be found, as was explained in Section

2.3, although this operation point can be found by increasing the bias current until the amplitude no longer grows with the bias current.
The reasoning for this is still that the main focus is on the MOS-varactor, and its capacitance characteristics.
Variation in the LC-tank VCOs output frequency due to two different amplitude values, is shown in Figure 4.8.

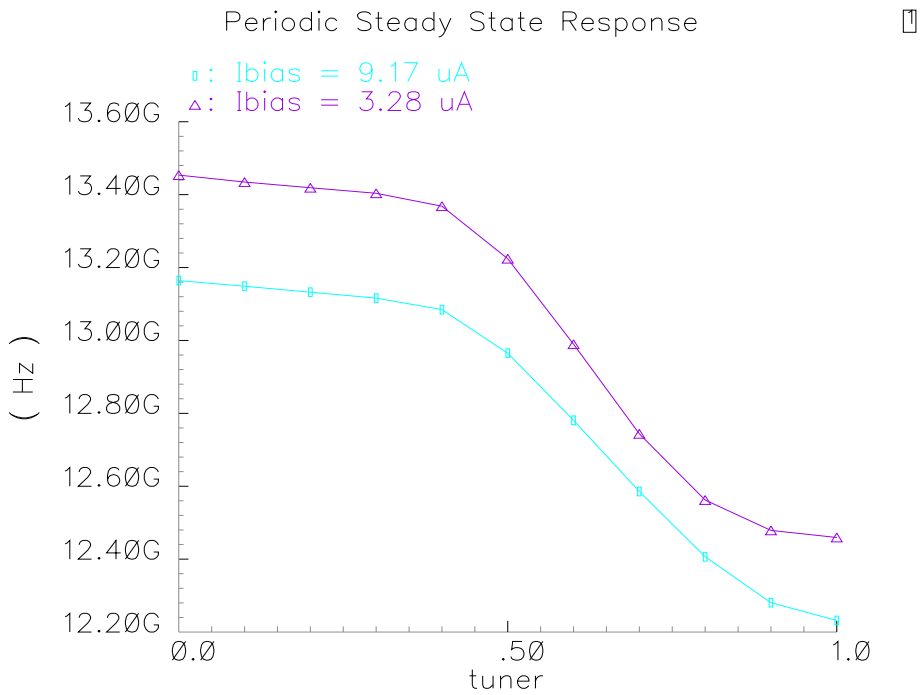

Figure 4.8: Change in VCO output frequency due to different amplitudes that are set by the bias current.

Further, an phase noise analysis also demonstrates the impact of the two amplitude values on the output frequency, seen in in Figure 4.9. The close-in phase noise is steadily a bit lower for the 428 mV amplitude, and it stays that way up to around 300K.The resulting phase noise values are quite high compared to works that specifically address the phase noise issue, for the 428 mV ampli-

Table 4.1: Different values of the output amplitude, set by the bias current.

$Width(\mu m)$	$Length(\mu m)$	$Bias-current(\mu A)$	$Max-amplitude(mV)$
5	0.2	16.58	608
5	0.5	9.17	526
5	1.5	3.68	428

tude, the phase noise was -4.172 dBc/Hz at 1K, at 10M it was -109.1 dBc/Hz. The 526 mV amplitude displayed -1.78 dBc/Hz at 1K and -112.1 dBc/Hz at 10M.

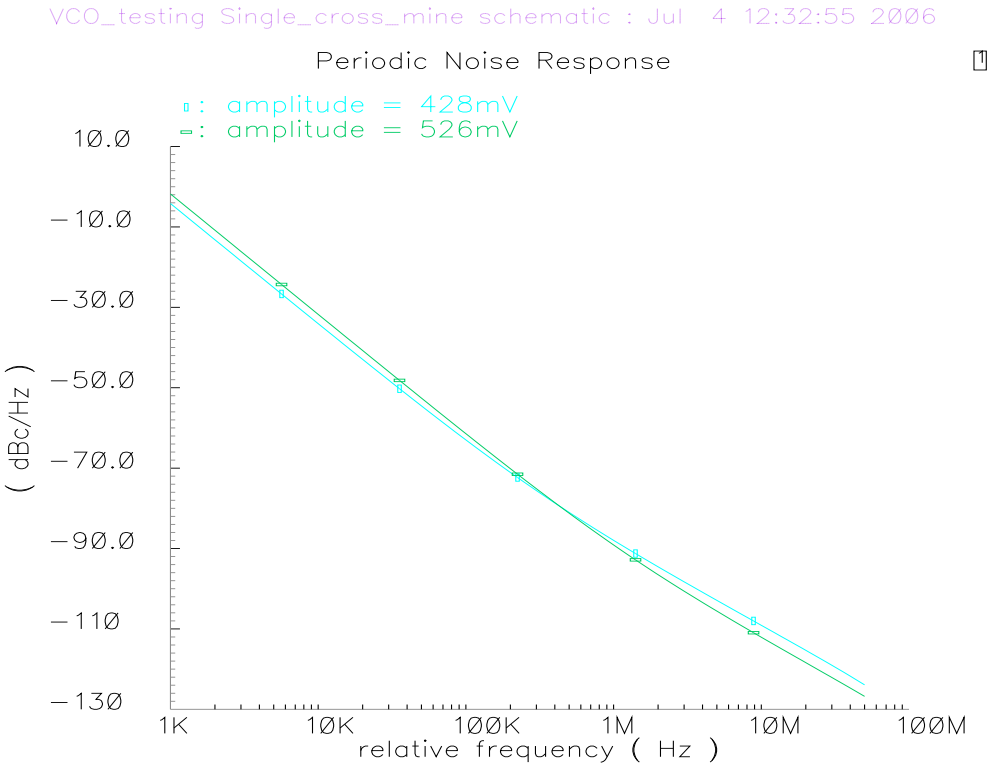

Figure 4.9: Change in phase noise due to amplitude variation with the bias current.

In Figure 4.10 the VCO output waveform is shown as a periodic signal, but not as a pure sinusoid. The shape of the waveform can be explained as follows: when the amplitude swing drives the capacitor toward the inversion region, its capacitance increases and the period of the oscillation slows down. When the varactor is pushed in the direction of the depletion region, the capacitance lowers and the period shortens.
The fact that positive and negative peaks with respect to the dc value have different magnitude is due to charge balance, between the two varactors that are coupled together, in the VCO. At each peak, one of the varactor reaches its maximum value, while the other one reaches its minimum. Since the charge conservation must hold, the voltage peaks are different. High capacitance corresponds to a reduced peak magnitude, and vice versa.

An higher amplitude swing increases the SNR ratio, and can improve the

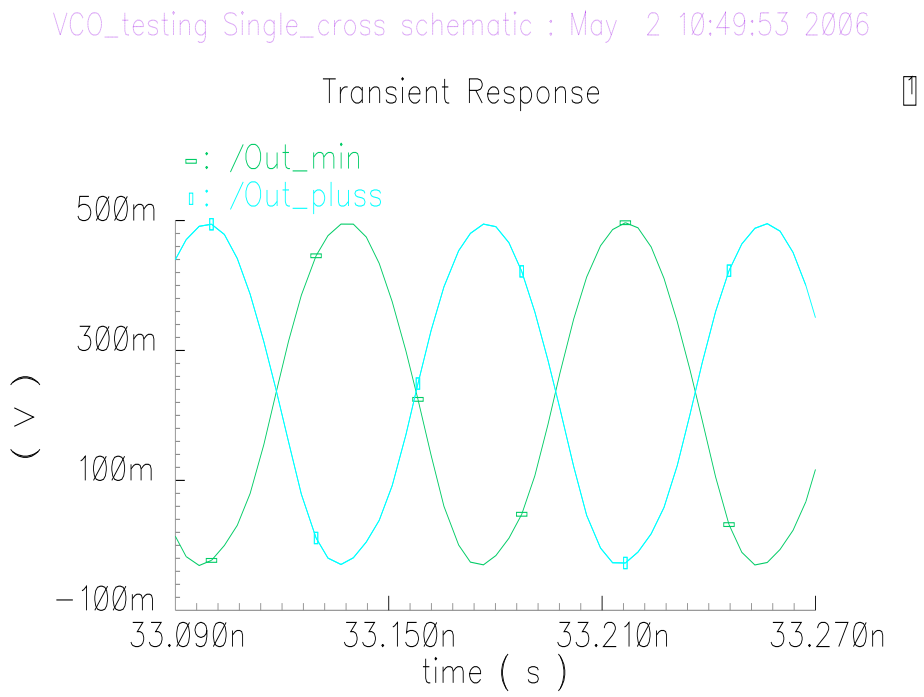

Figure 4.10: LC-tank VCO output waveform.

phase noise resulting from thermally induced noise sources, such as the active elements of the LC-tank VCO. On the other hand, increasing the amplitude swing will increase the AM-FM modulation, since the varactor capacitance is increasingly varied over the amplitude swings. This factor also contributes sidebands to the resonance frequency, which essentially is phase noise.

4.3 Linearity in the IMOS and NBG-varactors

To improve on the capacitance to frequency transition in the LC-tank VCO, an attempt was made to find approximately linear portions of varactor tuning curves. Obviously, it is important to have linear capacitance curve, with an wide as possible tuning range, if the output frequency is to follow Equation (1.1).
For this purpose both the IMOS and the NBG-varactor capacitance curves were closer examined, and implemented in the LC-tank VCO. The varactor dimensions where kept the same with $w = 5\ \mu m$ and the length was set at $l = 0.1\ \mu m$, with a 20 finger structure, in order to keep the Q-factor high and therefore having less resistive loss.
The output amplitude was set by the bias current and kept at the lowest amplitude value according to Table 4.1, around 428 mV. This way the AM-FM

modulation is kept low.

In Figure 4.11 the IMOS-varactors capacitance curve is shown, where V_{tune} is tuned 100 mV at a time, starting at 0.3 V and finally ending at 0.9 V. By stepping 20 steps for each 0.1 V of tuning, which is not much, this is a qualitative view of the capacitance characteristics.
This tuning region includes flat portions and also the steepest portions of the varactor capacitance curve.
Also seen for the different tuning voltage regions, is the capacitance derivative, which represents the rate of change.

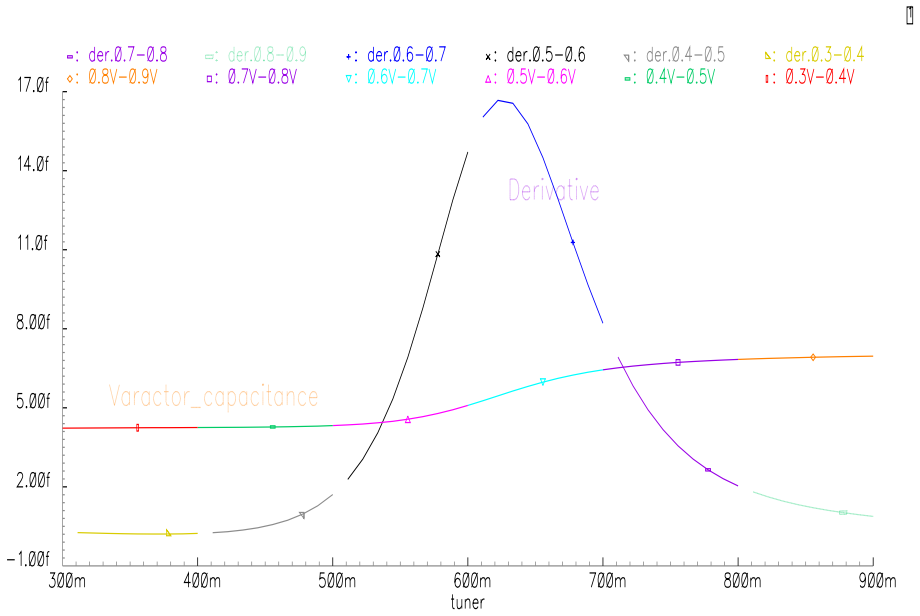

Figure 4.11: The derivative of the IMOS-varactor capacitance curve.

The derivative of the IMOS-varactor capacitance curve is seen to be higher than zero, and positive, indicating that the capacitance curve is increasing with V_{tune}. The derivative should ideally be a constant value, since this will indicate a linear tuning region. However, if the derivative is constant zero, this would indicate that the capacitance is not changing with the tuning voltage, in other words, zero frequency tuning occurs.

The NBG-varactor capacitance curve and its derivative are displayed in Figure 4.12, where V_{tune} was tuned from 0 to -0.9 V. As the NBG curve is declining in this tuning region, its derivative has a negative value.

In Figure 4.4 both the IMOS and NBG varactor structures display a fairly flat and slow changing capacitance characteristic around the 0 to 0.2 V tuning

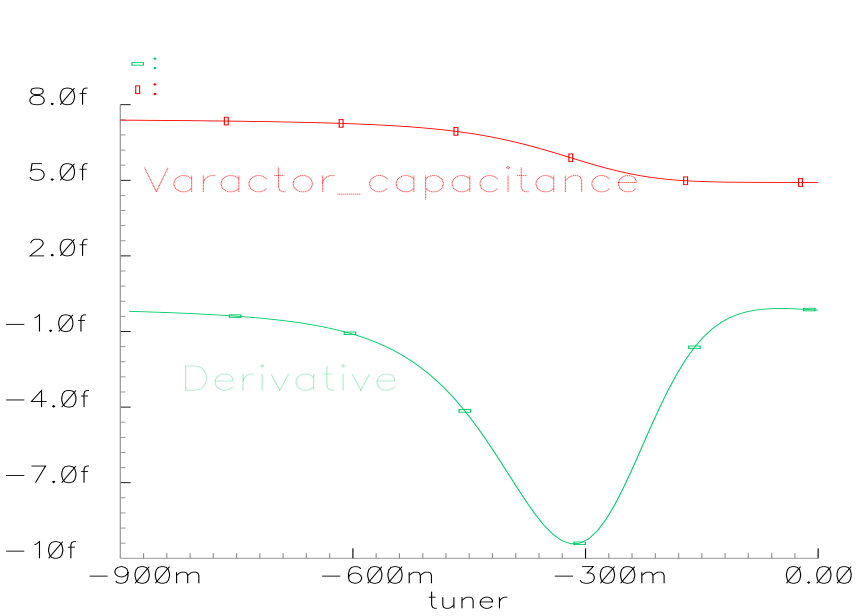

Figure 4.12: The derivative of the NBG-varactor capacitance curve.

voltage region. The IMOS-varactor is seen to be slowly rising, while the NBG-varactor is slowly declining. It is interesting to see which of the two structures is the most linear in that voltage region. The capacitance curves and the derivative of the IMOS and the NBG varactors for that particular tuning voltage region, are zoomed in and plotted in Figure 4.13. The values obtained from the varactors can be seen in Table 4.2.

Table 4.2: Derivatives of the IMOS and NBG-varactors, in the $V_{tune} = 0$ - 0.2 V region.

$V_{tune}(V)$	$Cap.IMOS(fF)$	$Deriv.IMOS(aF)$	$Cap.NBG(fF)$	$Deriv.NBG(aF)$
0	4.0806	551.35	4.9540	-2.5316
0.05	4.1091	588.48	4.8849	-735,78
0.1	4.1389	596.57	4.8673	-178.97
0.15	4.1674	539.50	4.8610	-119.97
0.2	4.1925	465.97	4.8534	-181.84

As the IMOS-varactor is displaying less change in its derivative, compared to the NBG-varactor, it has higher linearity, at least for that particular tuning region. This was confirmed by using the curve fitting tool in the handy Matlab environment.
A linear polynomial fit was used to more closely determine the linearity, as

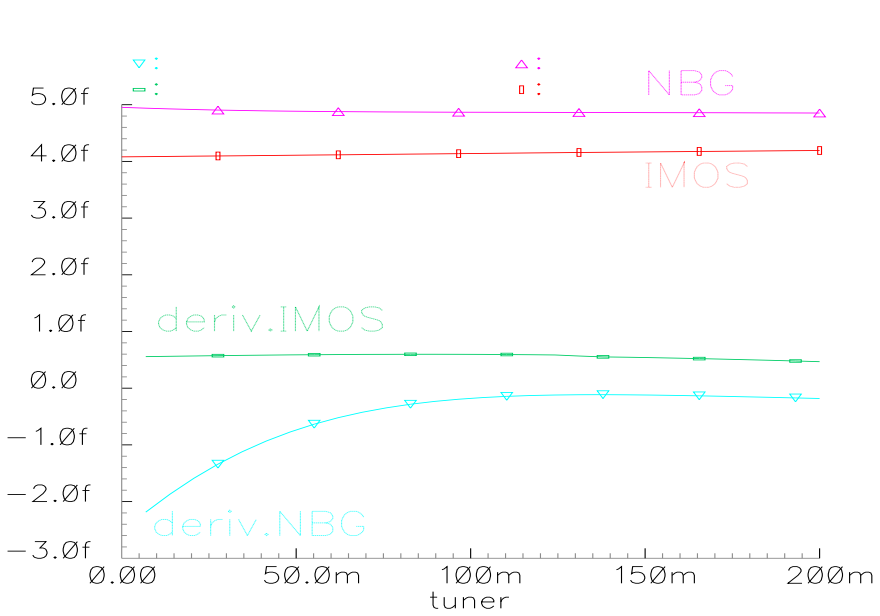

Figure 4.13: The IMOS and NBG varactor capacitance curves and their derivatives, in the V_{tune} = 0 - 0.2 V region.

seen in Figure 4.14.

There was a significant difference in linearity for the two varactors, with the IMOS-varactor displaying significantly higher linearity, which can be seen from the data in Table 4.3.

The goodness of fit statistics are as follow:

Table 4.3: Linearity of the IMOS and the NBG-varactors in V_{tune} = 0 - 0.2 V region

GoodnessOfFit	*IMOS*	*NBG*
SSE	5.094e-35	8.605e-33
R-square	0.9992	0.7621
Adjusted R-square	0.9992	0.758
RMSE	9.372e-19	1.218e-17

- SSE – The sum of squares due to error. This statistic measures the deviation of the responses from the fitted values of the responses. A value closer to 0 indicates a better fit.
- R-square – The coefficient of multiple determination. This statistic measures how successful the fit is in explaining the variation of the data. A

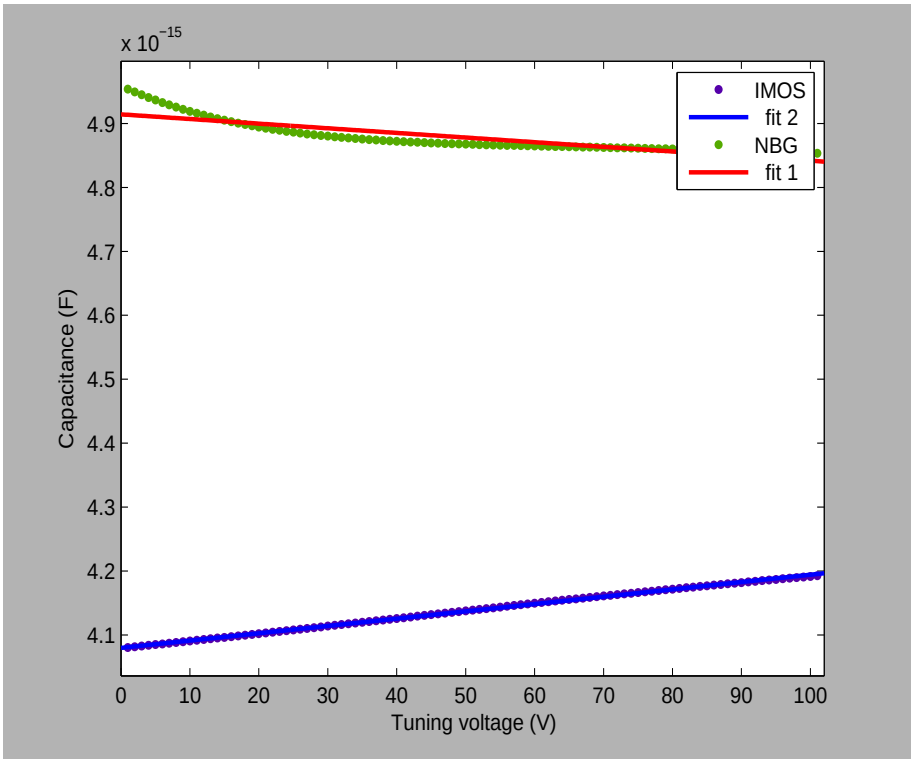

Figure 4.14: Linear fitting of the IMOS and NBG-varactors, in the $V_{tune} = 0$ - 0.2 V region.

value closer to 1 indicates a better fit.

- Adjusted R-square – The degree of freedom adjusted R-square. A value closer to 1 indicates a better fit. It is generally the best indicator of the fit quality when you add additional coefficients to your model.

- RMSE – The root mean squared error. A value closer to 0 indicates a better fit.

From this demonstration, the IMOS-varactor is seen to have some fairly linear capacitance regions, but still the linearity needs to be valid over a wide and steeper capacitance region.

4.4 Summary

The purpose of this chapter was to get into the operation of the LC-tank VCO, with the MOS-varactor in focus, through schematics drawing and analysis of

simulation data. This way, some of the effects mentioned in the previous chapter where confirmed. Some explaining was provided to the decisions made, as to why they are meaningful for this work.
Different MOS-varactor structures and capacitance regions were tuned, and some of the effects mentioned in the **Variable capacitance tuning** chapter, such as the amplitude swing impact, were seen through simulations and plots.
The LC-tank VCOs frequency output resulting from the varactor tuning, and also plots from phase noise simulations were shown.
Finally, a comparison was made between the IMOS and NBG-varactor, where the linearity of the two varactor was derived. This resulted in the IMOS displaying the most promising performance of the two.
This chapter provides some practical background and tools for the next chapter, in which the main contribution of this work is presented.

5 Improved performance utilizing varactor combinations

As seen from this thesis so far, there are limited ways to improve on the capacitance characteristics of the MOS-varactors. Therefore, one obvious question comes to mind: how can these characteristics be influenced in a simple and useful way?
One solution not seen utilized during the information gathering on the subject of varactors and LC-tank VCOs, is to use two or more MOS-varactors with different capacitance tuning characteristics, place them in parallel, still using a single tuning voltage, and then examine the usefulness of the resulting capacitance characteristics.
This chapter deals with the possibilities provided by the parallel combined varactor structure.

In addition to the MOS-varactors displayed in the previous chapter, a couple of others were configured, these are shown in Figure 5.1.
Each varactor device is based on either a nMOS or pMOS transistor, with various connecting combinations, that define their individual tuning characteristics.

These MOS-varactor devices display different changes in their capacitance characteristics over different parts of the applied tuning voltage, some are growing, while others are declining, as seen in Figure 5.2.

For the MOS-varactors shown in Figure 5.1, yet other capacitance characteristics can be obtained. This can be done by using different connections than those shown, between the tuning voltage, the supply voltage, GND, and the varactor source, drain and bulk terminals. For instance, one combination is to apply the tuning voltage at source and the drain simultaneously, while another combination is to apply the tuning voltage on only one of the terminals, either the source or the drain.
However, it is important to keep in mind effects such as when a transistor is working in saturation, then the potential variation at the drain region does not influence the channel charges [14].

The interesting part is to combine these different MOS-varactors, and see the resulting capacitance curves. The M4-varactor capacitance curve is plotted two times in Figure 5.2 using the same minimum length 0.1 μm both times, but with two different widths. The light blue coloured curve was obtained using

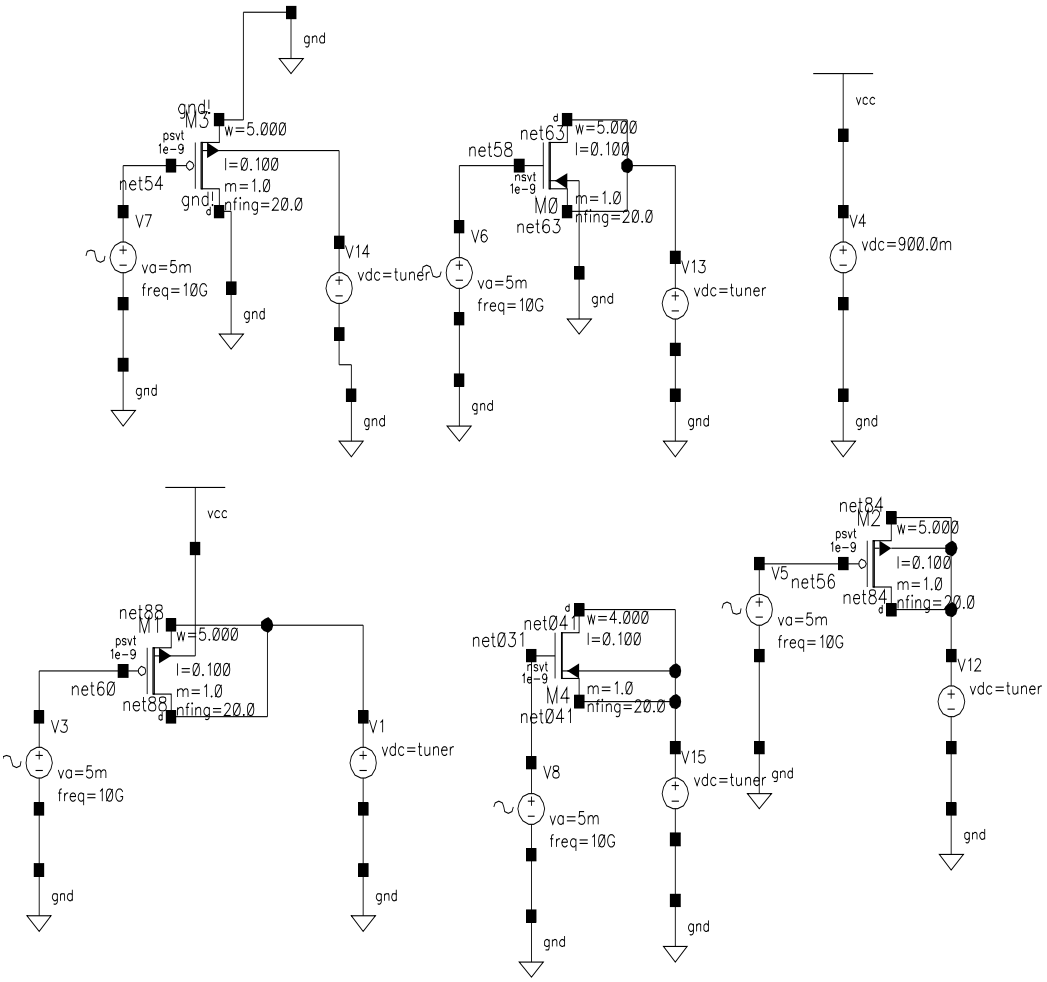

Figure 5.1: Different MOS-varactor structures.

$w = 4\ \mu m$, while the orange coloured curve was obtained using $w = 5.2\ \mu m$. This demonstrates how the capacitance curves are shifted relative to each other.

Assuming two parallel coupled MOS-varactors in approximately the same capacitance region, where one capacitance curve is climbing while the other is declining, there will be a summing, resulting in a new capacitance curve, which is essentially an averaging of the two.
The varactor with the highest capacitance derivative will dominate the changes in the resulting capacitance curve. With alignments and combination of the different capacitance curves, an efficient way of influencing varactor character-

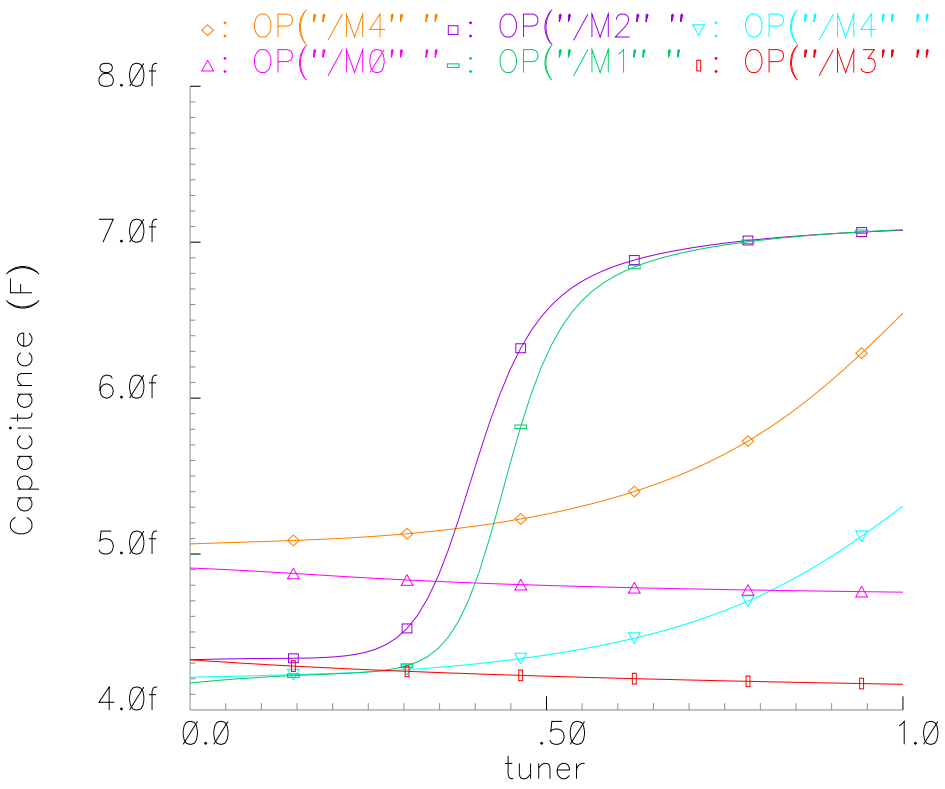

Figure 5.2: Several interacting small-signal capacitance curves.

istics is provided.
By combining varactors, there is also the possibility that one can have a similar effect on the resulting capacitance curve as was seen obtained with differential multi-finger gate doping in Section 3.4.
As mentioned there, the mixed gate doping of the varactor gates resulted in a flatter and more linear capacitance curve across the gate swing. This was due to the averaging of the most negative and the most positive doped finger gates. By combining two equally sized and identical configured MOS-varactors in parallel, where the only difference between them is that one has positive gate doping, while the other has negative doping, the sum of the two varactor capacitance curves will display approximately the same characteristics as the differential doped varactor gate in Figure 3.8. Also, as a result of this summing of the two capacitance curves, the output frequency will decrease and be shifted

down according to:

$$\omega_{osc} = \frac{1}{\sqrt{L * (C_{pos.gate}(V) + C_{neg.gate}(V)}}. \tag{5.1}$$

Therefore, if there are negative and positive doped transistor gates available, there is the possibility to combine them, and cancel out the need of a transistor with mixed gate doping in order to get increased linearity.
This approach in order to increase the linearity of the MOS-varactor, may be better, or perhaps worse than using the mixed gate doping, but no further work was done to compare the two.
However, the cancelling characteristics of the combined varactors should not be left out, which might even be improved on by using specific gate doping profiles in order to make the cancelling effect become more efficient.
Anyhow, the important thing is to gain some control over the varactor capacitance curves, so that capacitance lying across the LC-tank VCOs amplitude swings becomes more evenly distributed. This provides the possibility for the LC-tanks output frequency to increasingly perform according to the inverse square law, opening up the possibilities provided through the intended digital correction.

5.1 Constant derivative

In mathematical terms, the derivative is defined as the instantaneous rate of change of a function. When two capacitance curves are placed together, where one is rising, while the other one is declining, and their magnitudes of change are equal, then their derivatives will display a cancelling action. As a result, the derivative of the resulting capacitance curve will be a constant, and the capacitance curve will display a linear behaviour with the tuning voltage.
In Figure 5.3 an illustration of the ideal linear capacitance curve resulting from the cancelling action, is shown. Also, the similarity of one of the combined capacitance curves to that of the IMOS-varactors capacitance curve, should be noticed.
The slope at which the resulting capacitance curve is rising/declining is important, since it will determine the frequency tuning range, and it also impacts the tuning voltage sensitivity of the LC-tank VCO. Therefore, it is important to align the cancelling capacitances correctly, so that they provide the desired slope for the resulting capacitance curve.
By using gate doping, there is the possibility to try to adjust the slope of the resulting capacitance curve, perhaps by shifting the flatband voltage. However, since this is related to physics in the transistors, it is not something that was tried out in this thesis.

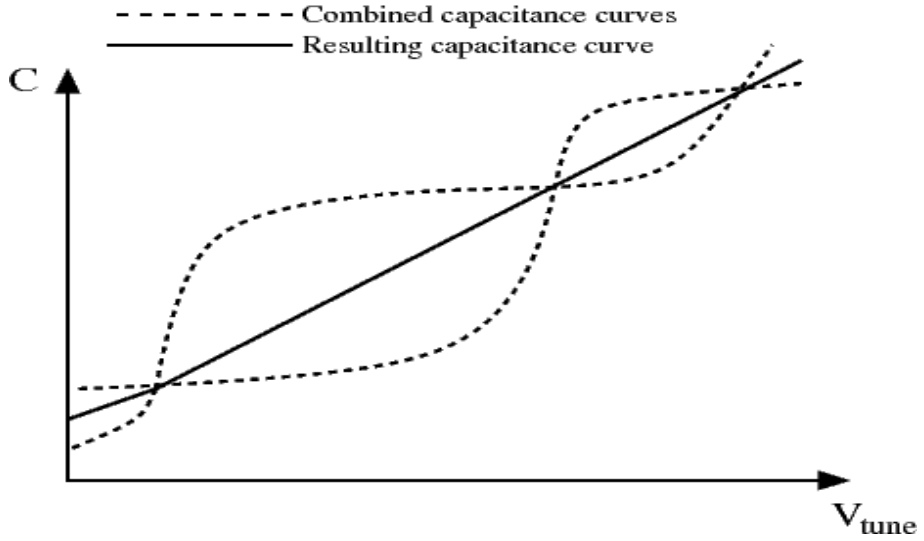

Figure 5.3: Illustration of ideal derivative cancelling principle.

The mathematical expression

$$A * X + B \tag{5.2}$$

describes a linear function, and it can be used to describe the capacitance curve resulting from an ideal cancellation. If the derivative of the resulting capacitance curve is a constant, it can be set equal to A, which will be represent a constant rate of change for the capacitance curve. The X factor will be representing the incremental tuning voltage. The B factor will express the capacitance region of operation, and therefore the initial value of the resulting capacitance curve, determined by the two compensating capacitance curves.
Curve fitting tools can be applied to take measurements of the characteristics of the MOS-varactor, such as the improvement in linearity gained from the derivative cancellation of the combined MOS-varactors.

5.2 Combined MOS-varactor frequency tuning

To see the actual impact of the combined MOS-varactors on capacitance and the output frequency, the IMOS and the M4 varactor devices from Figure 5.1 were combined and implemented in the LC-tank VCO. The M4 varactor, representing a nMOS transistor with the tuning voltage applied at the source/drain and the bulk terminals, will from here on be called the NDSB-varactor for simplicity.

Figure 5.4 shows the combined IMOS/NDSB varactor structure, where the

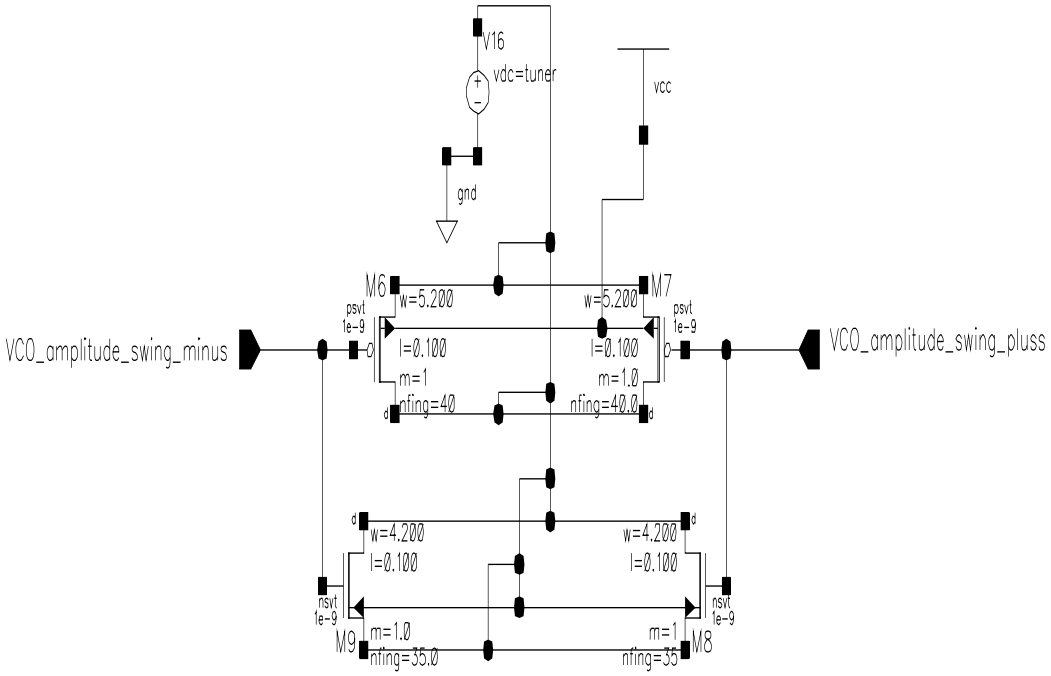

Figure 5.4: The parallel combined IMOS/NDSB-varactor.

IMOS-varactor dimensions are a $w = 5.2\ \mu m$, $l = 0.1\ \mu m$ and 40 fingers, while $w = 4.2\ \mu m$, $l = 0.1\ \mu m$ is used for the NDSB, with a 35 finger structure.
The maximum output amplitude swing was set by the bias current at 428 mv, which is the lowest amplitude value in Table 4.1, since this will provide low AM-FM modulation.
The individual capacitance curves of the IMOS and the NDSB varactor are displayed in Figure 5.5.

In the simulation environment used, the capacitance curve resulting from the combined MOS-varactors, could not be plotted in the same way as the individual varactors, simply because there is no gate to represent the resulting gate oxide capacitance. This however, is not a concern when plotting the LC-tank VCOs output frequency, since it is determined by the summed capacitance.
A couple of things should be kept in mind when running the periodic state(PSS) analysis, where the harmonic analysis provides the plots of the output frequency as a function of the tuning voltage. It is important to keep the stabilisation time high during the PSS analysis. By keeping the stabilisation time too

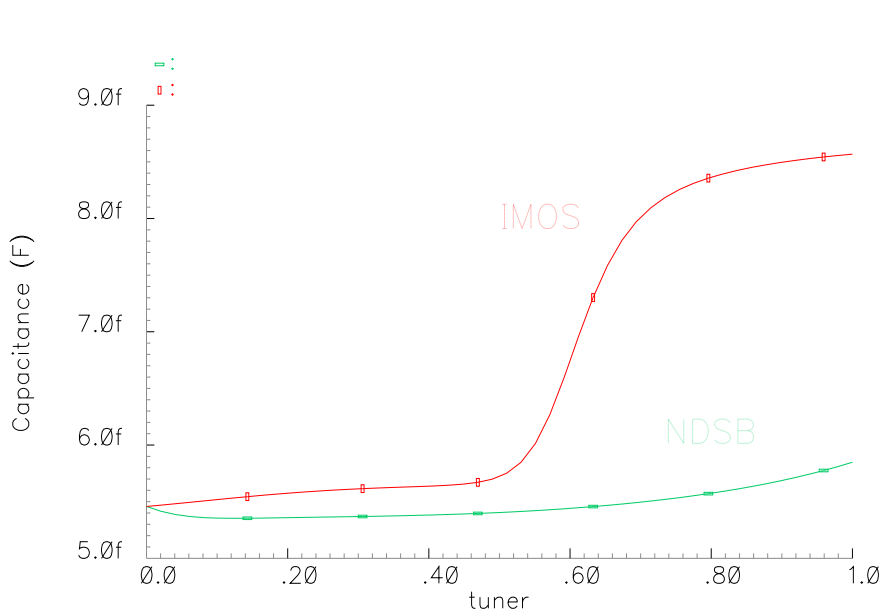

Figure 5.5: IMOS and NDSB capacitance curves.

low, the output frequency curve will display an uncontrolled behaviour, since it wont have enough time to settle properly. In this case, the TSAB stabilisation time was set at 400 nS, which was more than sufficient. Also, in order to avoid other problems, the beat frequency in the PSS analysis should be kept lower than the maximum output frequency. In this case the LC-tank VCO generates an output frequency approaching 13 GHz, therefore, the beat frequency was set at 10 GHz.

The impact of the combined IMOS/NDSB-varactor on the LC-tank VCOs output frequency, is seen in Figure 5.6. Also, the frequency output from using the single IMOS-varactor and the single NDSB-varactor are shown in Figure 5.6.
The frequency curves is seen to be different then the ideal displayed in Equation (1.1), the reason for that is obviously that the frequency is shown as a function of the tuning voltage, and not the capacitance.
The IMOS-varactor displays a frequency range going from 12.01 to 12.96 GHz, while the NDSB displayed a frequency range going from 12.81 to 12.99 GHz. The results from combined IMOS/NDSB-varactor, was a frequency range of about 750 MHz, going from 10.66 to 11.41 GHz.
In this case, it is seen that the frequency range for the combined structure was approximately 100 Mhz less then that obtained from the single IMOS-varactor.

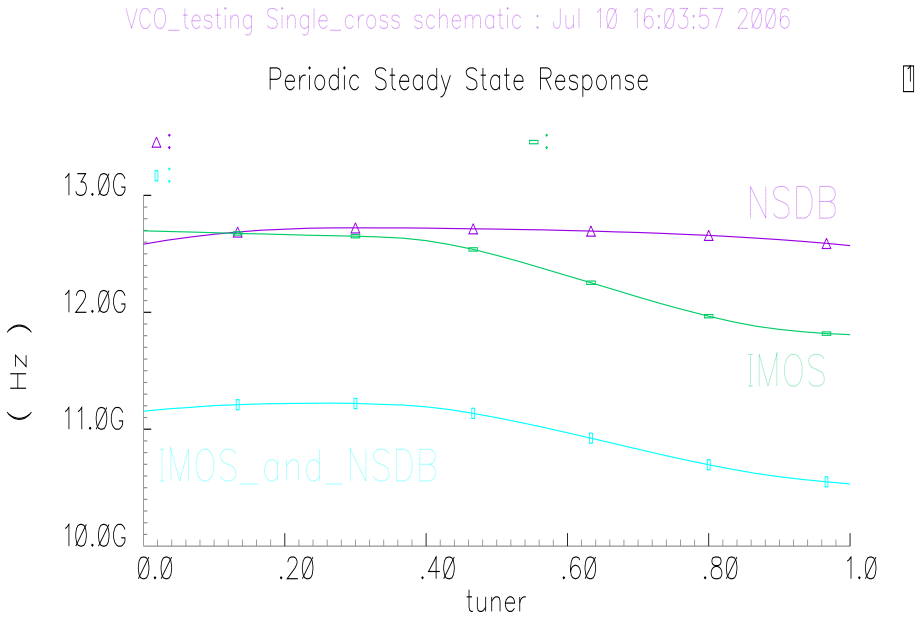

Figure 5.6: The combined IMOS/NDSB-varactors impact on the LC-tank VCOs output frequency curve.

5.3 Improved linearity and tuning range

In this section the potential of improvement in the LC-tank VCOs frequency tuning, that is provided by the combined varactors, will be demonstrated. A portion of the combined IMOS/NDSB-varactors capacitance curve is closer examined, and it is shown that both the linearity and the capacitance tuning range is improved.

As seen in Figure 5.5, around the 0.8 - 1 V tuning voltage region the NDSB and the IMOS-varactor capacitance curves are oppositely growing and declining. Therefore, the linearity of the two individual capacitance curves, and also the linearity of the resulting, summed capacitance curve, was measured using linear fitting tools.

Linear fitting plots are shown in Figure 5.7, while the corresponding linearity data is collected in Table 5.1.
Improvements in linearity can be seen in the combined IMOS/NDSB capacitance curve, in addition the available capacitance over that particular tuning voltage region has increased. The resulting capacitance curve in Figure 5.7 is seen at a higher capacitance level than the IMOS and the NDSB-varactor curves, due to the summing effect.

The idea of using two capacitance curves to form a single one, is most effec-

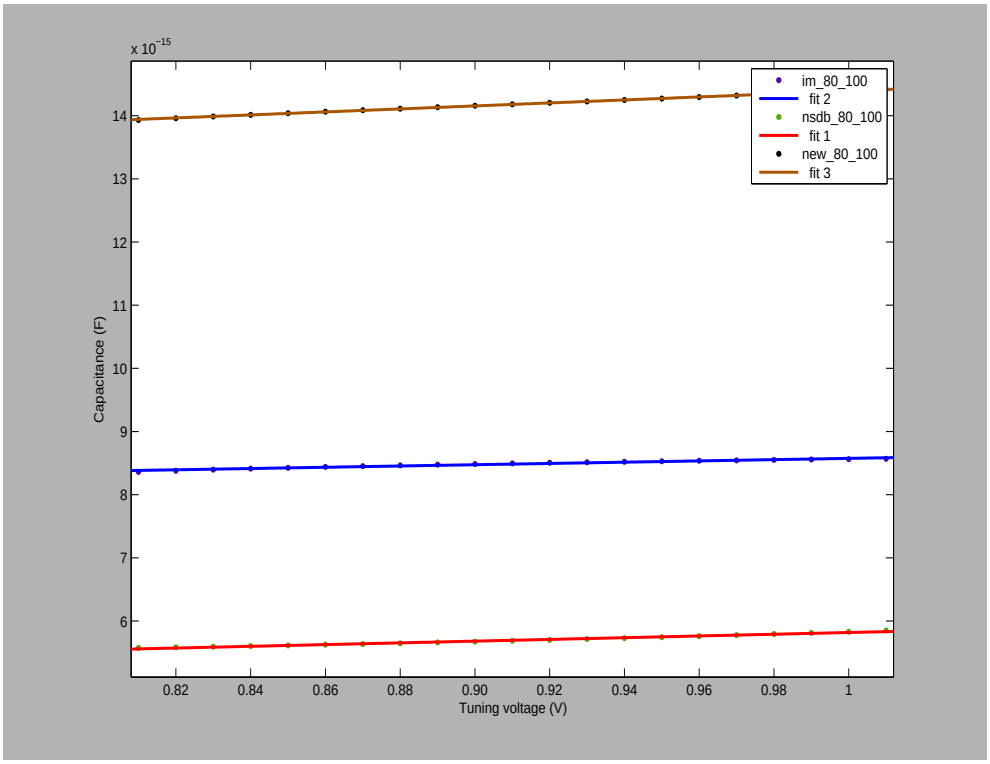

Figure 5.7: Linearity and tuning range improvement with the combined IMOS/NDSB-varactor in $V_{tune} = 0.8$ - 1 V region.

Table 5.1: Linearity and tuning range improvement with the combined IMOS/NDSB-varactor in $V_{tune} = 0.8$ - 1 V region.

$GoodnessOfFit$	$IMOS$	$NDSB$	$IMOS/NDSB$
SSE	2.222e-33	1.399e-33	1.89e-34
R-square	0.9722	0.9904	0.9996
Adjusted R-square	0.9707	0.9898	0.9995
RMSE	1.081e-17	8.581e-18	3.154e-18
$Frequency(GHz)$	$IMOS$	$NDSB$	$IMOS/NDSB$
min	12.0196	12.8086	10.6638
max	12.101	12.913	10.787
range	0.0814	0.1044	0.1232

tive if the cancellation provided by the combined varactors, is effective over a wide tuning voltage range. In Figure 5.2 it is seen that the orange capacitance curve obtained by setting the width of the NDSB-varactor to $w = 5.2\ \mu m$, would probably have increased the linearity over an even wider voltage tuning range

than that used in Table 5.1. On the other hand, it might be difficult to find two ideal cancelling capacitance curves, particularly over the whole of the tuning voltage range.
Therefore, an alternative is to target smaller parts of the capacitance curves, as it is always easier to obtain linearity over smaller regions. As an example, lets assume an IMOS-varactor capacitance curve is tuned from $V_{tune} = 0$ - 1 V, displaying all three of its distinct capacitance tuning regions, C_{min}, C_{max} and the steep transition part.
Over these different capacitance regions, there is the possibility to use three different and individual varactors, with their own cancelling characteristics, and combine them at the right moment with the IMOS-varactor tuning curve.
This approach can provide linearity improvement over a wide tuning voltage range.
Obviously, this approach requires some control or switching schemes, in order to provide the proper combination and cancelling at the right moment. This will complicate matters, even if a single tuning voltage is still used. In addition, since several varactor combinations are used in this approach, the power dissipation will be increased, which is not favourable for the FDSM system.

5.3.1 Improved AM-FM performance

In Figure 3.7 approximately zero AM-FM modulation was shown in the slow varying and flat parts of the MOS-varactors capacitance curve. This zero AM-FM behaviour was due to the capacitance being evenly distributed across the LC-tank VCOs amplitude swings.
Unfortunately, the frequency tuning ranges are severely limited over these zero AM-FM and flat capacitance regions.
Also, approximately zero AM-FM modulation was found in the middle of the steep C_{max} to C_{min} transition region. This zero AM-FM modulation was seen to be the result of the time averaging effect of the evenly distributed C_{min}, C_{max} capacitances over the amplitude swing.
This time averaging can also be considered as a cancelling effect, since the C_{max} capacitance will makes sure the LC-tank VCOs waveform slows down, while the C_{min} capacitance makes sure it increases.

As explained in the previous section, the linearity and capacitance tuning range of the combined varactor structure may potentially be adjusted to a desired level. If a straight line with desired slope is obtained, the zero AM-FM condition will stay valid over a much wider frequency tuning range.
This relation is illustrated in Figure 5.8. For an rising/falling capacitance curve that is linear over a wide tuning voltage range, the relation between the C_{low} and C_{high} capacitances, that is distributed evenly across the amplitude swings, will stay constant. This means that there is an equal amount of change in the output frequency, for incremental steps of the applied tuning voltage, as long

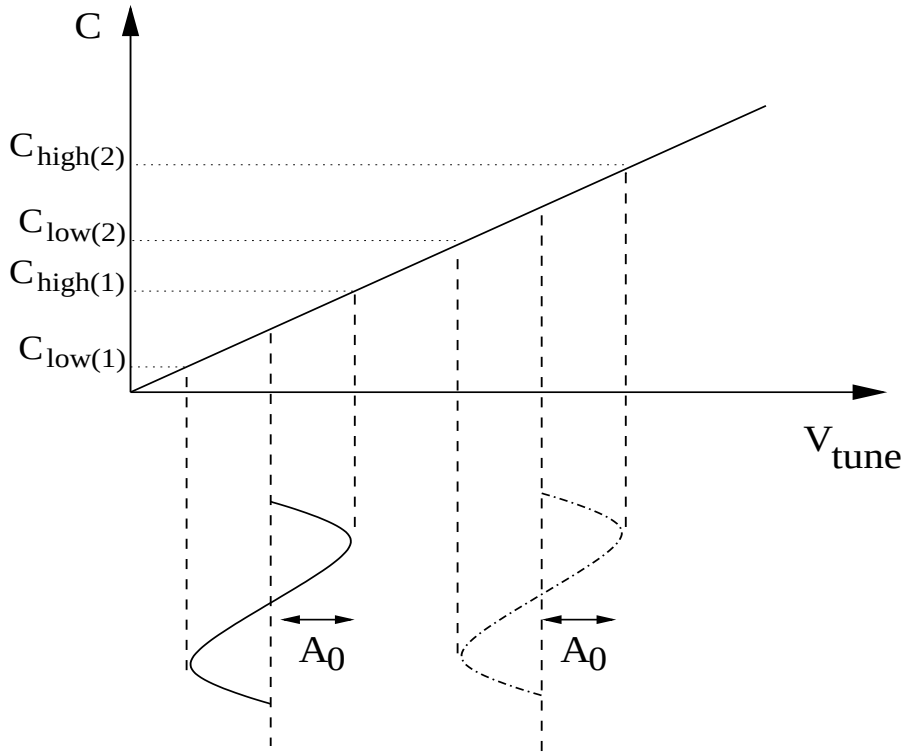

Figure 5.8: Illustration of a wide capacitance tuning range where zero AM-FM modulation takes place, due to linearity improvement

as the C_{low}, C_{high} criteria is valid.
In Figure 5.8 this principle is illustrated for two values of the tuning voltage,

$$A_o = C_{high(2)} - C_{low(2)} = C_{high(1)} - C_{low(1)}, \tag{5.3}$$

where the amplitude A_0 is assumed to be constant.

Obviously, in this case it is important to consider the magnitude of the LC-tank VCOs output swings, compared to the available tuning voltage range.
As an example, if the magnitude of the output swing is kept constant at 400 mV, perhaps by removing the bias current and making sure the output amplitude is set constant at 400 mV [15], over a tuning voltage range from 0 to 1 V, there will be a 600 mV tuning voltage range were the C_{low} and C_{high} relation continually stays the same.
Of Course, this reasoning is an simplification, since there is bound to be some AM-FM modulation as long as the capacitance curve displays nonlinear behaviour, and the amplitude is varied by different sources, such as the bias current and the supply voltages.

The factors mentioned in this section, such as the frequency range, the linearity, the zero AM-FM modulation and the tuning sensitivity, should all be taken into consideration, in order to provide the desired inverse square law frequency tuning from the LC-tank VCO.
Also, if an small amplitude swing is found at the oscillator output, an important trade off needs to be considered.
Since the FDSM system may operate with very low power, a small oscillator output amplitude will be favourable. However, a small output swing amplitude will degrade the SNR ratio, and this will cause the phase noise contributions to increase significantly.
By using a tuning voltage with a range that is larger than the magnitude of the oscillator output swing, the tuning voltage becomes the low-power-operation limiting factor. In the example mentioned above, the tuning voltage range was significantly larger than the signal magnitude, in order to demonstrate the large frequency range with zero AM-FM conversion, that is obtained from the improved linearity.
Obviously, if a small tuning voltage is used, the tuning sensitivity needs to be kept the lowest possible, in order to obtain high resolution in the FDSM system. In the next section, the AM-FM modulation and its contribution to the phase noise in the LC-tank VCO is considered.

5.4 Phase noise improvement

The phase noise characteristics of the LC-tank VCO from using the single IMOS-varactor was shown in Figure 4.9 for two different amplitude values.
To get a comparison with the combined IMOS/NDSB-varactor, another phase noise analysis was performed, with the same amplitude values. For the combined varactor, the IMOS-varactor dimensions where kept at $w = 5.2\ \mu m$, $l = 0.1\ \mu m$ with an finger structure of 40, while the other part, the NDSB-varactor, was given $4.2\ \mu m$, $l = 0.1\ \mu m$ and finger structure of 35.
The phase noise results obtained from using the combined IMOS/NDSB-varactor in the LC-tank VCO, are plotted along with the results from using the single IMOS-varactor, as seen in Figure 5.9.

From the data in Table 5.2 the phase noise shows improvement with the combined varactor structure, compared to the results from using the single IMOS-varactor. This would seem contradictory to what one would expect from using more than one varactor, since additional parasitic resistance is added, that reduce the LC-tank VCOs Q-factor.
Thus, by combining two varactors using the minimum length, it looks like the added parasitic resistance does not degrade the phase noise more than the improvement that is gained from the reduced AM-FM modulation.
Since the phase noise is not the main focus of this thesis, no further work was

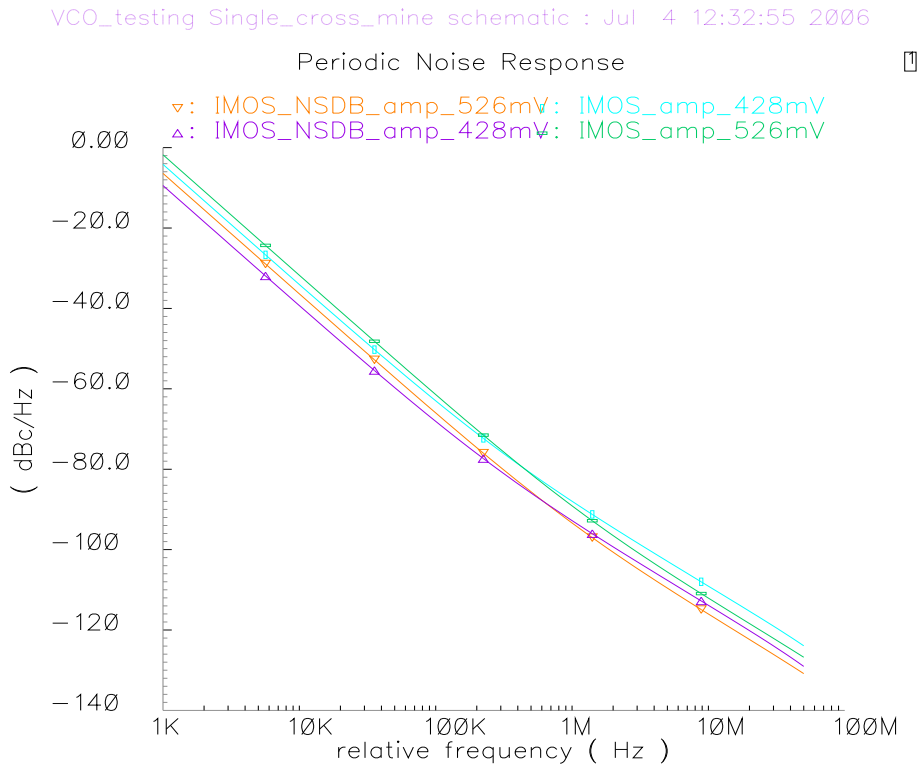

Figure 5.9: Phase noise performance when using the IMOS/NDSB-varactor, compared to using the single IMOS-varactor.

Table 5.2: Improvement in the phase noise performance from using the IMOS/NDSB-varactor compared to the single IMOS-varactor.

$Amp.swing(mV)$	$pha.offset$	$IMOS-NDSB(dBc/Hz)$	$IMOS(dBc/Hz)$
428	1K	-9.436	-4.172
428	10M	-113.9	-109.1
526	1K	-6.412	-1.782
526	10M	-116.1	-112.1

done to verify this statement. Also, from figure 5.9 it is seen that the amplitude value of 428 mV, that was obtained from setting the length of the bias current source to $l = 1.5\ \mu m$ (Table 4.1), is displaying lower phase noise characteristics from 1 to approximately 400 KHz, than the higher 526 mV amplitude swing. Clearly, this phase noise behaviour is something that should be looked into in a future work concerning the combined varactor structure.
Another trade-off that should be mentioned at the end of this section, is that

by using minimum varactor lengths, the Q-factor will stay high, and the phase noise will be reduced, but at the same time the frequency tuning range will be severely reduced. Also, there will be some increase in the power consumption from the combined varactor structures, where some combinations might be more efficient than other. However, the power measurements are not performed in this work, since the increased power consumption is thought to be marginal with the added small sized varactor, such as is the case when the NDSB is combined with the IMOS in this work.

5.5 Summary

The possibilities that are provided in order improve on the LC-tank VCOs frequency tuning characteristics, by using combination of different MOS-varactors, with their resulting cancelling characteristics, was the focus of this chapter.
The combined IMOS/NDSB-varactor was used as an example, and tuned with a single tuning voltage. This combination displayed linearity improvement, and partially increase in the available capacitance tuning region. Improvements in the phase noise performance due to less AM-FM modulation, was also demonstrated, and some important trade offs to keep in mind were mentioned.

6 Conclusion and future work

The integrity of the information being handled in the FDSM system, needs to be optimized, therefore the integrated oscillator must maintain the linearity between the input voltage and the frequency output that it generates. Even before this thesis got started, an ring oscillator was designed intended for the FDSM system [24]. Since both the LC-tank and the ring oscillators have their own strong and weak sides, it is important to bring about means of comparing their performance in the FDSM environment, something this work hopefully will contribute to. In addition to the comparison part, this work provides an useful technique to improve on the LC-tank VCO frequency tuning characteristics, which amongst other things is known for its limited tuning range.

The LC-tank VCOs inverse square law (ISL) frequency tuning curve was seen in the introduction of this thesis, and the linearization possibility provided through digital squaring was mentioned. Strangely enough, this linearity providing approach has not been seen utilized in any of the literature on the frequency tuning of the LC-tank VCO.
On the other hand, it is not a straight forward task to provide the desired ISL-frequency curve at the LC-tank VCOs output either. This is partially due to the limited linearity in abrupt MOS-varactors, and also the large signal LC-tank VCOs amplitude swings, that modulate the output frequency. In addition, there are other phase noise contributing sources, such as the active compensating devices.
When an approximately linear but small MOS-varactor capacitance region is used to tune the LC-tank VCO, while a small amplitude swing is lying across it, the frequency output will display a fairly linear behaviour. This seemingly linear frequency curve, is only a small part of the overall ISL-frequency curve of the LC-tank VCO. Also, since the output frequency needs to be divided down to a FDSM compatible level, the frequency tuning range is severely reduced, removing some of the inverse square behaviour. Therefore, in order to obtain the desired ISL-frequency output a much wider, and still linear MOS-varactor region would be needed.

In the **Design and analysis of LC VCO using MOS-varactor** chapter, the linearity of the NBG and the IMOS varactor was compared over a flat capacitance region, with the IMOS displaying the best results. This lead to the utilization of the IMOS-varactor as one part of a combined varactor structure in the **Improved performance utilizing combined varactors** chapter. The other part

that was used in order to provide the desired cancelling characteristics, was the NDSB-varactor. The NDSB was obtained by testing and comparing several different MOS structures.
By tuning the IMOS/NDSB-varactor over the $V_{tune} = 0.8$ - 1 V region, improvement was seen in both the linearity and the tuning range, and also phase noise improvements were shown.
This clearly demonstrates the practical and theoretical possibilities from combining varactors in parallel, where means are provided to significantly improve on the frequency tuning characteristics of the LC-tank VCO.
When the LC-tank VCO is tuned with the combined varactors, and digital correction is applied, essentially two cancelling stages are used in order to get a linear input/output relation for the FDSM. In the first stage, linearity is increased in the capacitance tuning, with the cancelling action of the combined varactors. Then, the intended digital squaring of the output bits provides another cancelling effect on the the ISL-frequency curve. Unfortunately, the intended squaring was not performed at the time this thesis was reaching its finish, as it took more time than expected.

The idea of placing varactors in parallel, in order to increase the linearity in the LC-tank VCOs frequency output curve, is not new [25]. However, the technique described in this thesis, which provides a flexible way of combining different MOS-varactor capacitance curves, was not seen utilized in the literature.
By using only MOS-varactors, the tuning voltage may be swept across the full power supply, with no fear of forward biasing, something that can occur with the p+/n-well junctions varactors.
Also, the single tuning voltage avoids the control schemes needed when more that one tuning voltage is used, thereby simplifying matters.
The work in this thesis may be further improved, since there are several untested varactor combinations to be made. Even the promising AMOS-varactor, that was not available for this thesis, may be significantly improved with the varactor combination approach.
It would be interesting to see whether a single cancelling capacitance can be found, one that provides the desired capacitance curve across the whole of the voltage tuning range used.
Since the frequency tuning of the combined varactor in this work has not yet been optimized to the full, no real comparison of linearity or frequency range has been made with other works that have extensively targeted these issues. However, this work certainly provides the insight to further improve on the combined varactor technique.

The possibilities provided by the combined MOS-varactors, may potentially be useful in other areas of circuit design.
Therefore, it might be interesting for semi-conductor manufacturers to look

into the cancelling behaviour of the combined structures, if this is has not already been done. Having said that, the search for a single compensating capacitance curve may not be a trivial matter. Therefore, an alternative has been proposed in this thesis, where one MOS-varactor capacitance curve is used as a reference, while three different compensating varactors, with different capacitance curves, are switched in/out over specific parts of the reference capacitance curve. This way, the cancelling characteristics are provided more accurately where they may be needed.
This approach is starting to look similar to the switched tuning capacitor approach, where a wide frequency range can be obtained [26]. The challenge then becomes to build satisfactory RF switches, in order to select and combine the right varactors, at the right tuning voltage values. This approach would require several varactor combinations, therefore the power dissipation will increase, which is obviously not favourable for low power operating systems, such as the FDSM.
In this thesis, no such switching mechanism was designed, simply because there was not enough time to do so. Also, no measurements were made on the increased power consumption from using the combined IMOS/NDSB-varactor in this thesis. However, my guess is that the additional power consumption in this case is marginally. Another step that was left out due to time constraints, is the implementation of the designed LC-tank VCO with the combined varactor structure on a chip. This had to do with deadlines that kept changing several times, therefore this step was left out. Although it would have been interesting to measure and compare the result of a completed LC-tank VCO circuit, to those result that where obtained through simulations and other linearity measuring techniques. This certainly would be a prospect for future work on the combined varactor structure.
Also, it is important to mention that throughout this thesis, minimum length varactors have been used, in order not to degrade the Q-factor. In order to obtain an higher frequency tuning range, so that the ISL-frequency characteristics becomes more visible, varactor dimensions need to be increased. Therefore a functional trade off between the reduced Q-factor and the increased tuning region should be found.

Finally, there is even another LC-tank VCO frequency tuning option that should be mentioned, and perhaps even compared to the frequency curve from the yet to be optimized combined varactor structure. There is the possibility of obtaining the desired wide range ISL-frequency output, by using a variable inductor, with MEMS components incorporated into the frequency tuning [27].
The specifics of this approach has not been closer investigated in this thesis, since the inductance value of the LC-tank was kept constant throughout this work.

Bibliography

[1] Mats Høvin, Alf Olsen, Tor Sverre Lande, and ChrisToumazou. Delta-sigma modulators using frequency-modulated intermediate values. *IEEE Solide-State Circuit*, 32(1), January 1997.

[2] R. Norris. Lc tank voltage controlled oscillator tutorial. Technical report, Presentation to the UW ASIC Analog Group, Waterloo, Ontario, Canada, 2005.

[3] Yalcin Alper Eken and John P. Uyemura. A 5.9-ghz voltage-controlled ring oscillator in $0.18 - \mu m$ cmos. *IEEE Solide-State Circuits*, 39(1), January 2004.

[4] Cadence Design Systems. Vco design using spectrerf, application note. Technical report, Cadence, 2004.

[5] M. Tiebout. *Low Power VCO Design in CMOS*. Springer, 2006.

[6] Sangwoong Yoon. *LC-tank CMOS Voltage-Controlled Oscillator using High Quality Inductors Embedded in Advanced Packaging Technologies*. PhD thesis, Georgia Institute of Technology, 2004.

[7] Roberto Aparicio and Ali Hajimiri. A noise-shifting differential colpitts vco. *IEEE Solide-State Circuit*, 37(12), Desember 2002.

[8] Soenc C, Van der Plas G, Wambacq P, and Donnay S. Substrate noise immune design of an lc-tank vco using sensitivity functions.

[9] Giuseppe De Astis, David Cordeau, Jean-Marie Paillot, and Lucian Dascalescu. A 5-ghz fully integrated full pmos low-phase-noise lc vco. *IEEE Solide-State Circuit*, 40(10), October 2005.

[10] J. H. C. Zhan, J. S. Duster, and K. T. Kornegay. A comparative study of mos vcos for low voltage high performance operation. Technical report, Cornell University.

[11] Ali Hajimiri and Thomas H. Lee. Design issues in cmos differential lc oscillators. *IEEE Solide-State Circuit*, 34(5), May 1999.

[12] John W.M. Rogers, José A. Macedo, and Calvin Plett. The effect of varactor nonlinearity on the phase noise of completely integrated vcos. *IEEE Solide-State Circuit*, 35(9), September 2000.

[13] Donhee Ham and Ali Hajimiri. Concepts and methods in optimization of integrated lc vcos. *IEEE Solide-State Circuits*, 36(6), June 2001.

[14] Thomas H. Lee. *The Design of CMOS Radio Frequency Integrated Circuits*. Cambridge University Press, 1998.

[15] S. Levantino, C. Samori, A. Bonfanti, S. L. J. Gierkink, A. L. Lacaita, and V. Boccuzzi. Frequency dependence on bias current in 5-ghz cmos vcos: Impact on tuning range and flicker noise upconversion. *IEEE Solide-State Circuit*, 37(8), August 2002.

[16] E. Hegazi. Varactor characteristics, oscillator tuning curves, and am-fm conversion. *IEEE Solide-State Circuit*, 38(6), June 2003.

[17] Suman K. Banerjee, Yang Du, Rainer Thoma, and Alain C. Duvallet. Simulation and benchmarking of mos varactors for tha cmos090 rf process technology. Technical report, Motorola S^3 Symposium.

[18] R. L. Bunch and S. Raman. Large-signal analysis of mos varactors in cmos $-g_m$ lc vcos. *IEEE Solide-State Circuit*, 38(8), August 2003.

[19] Pietro Adreani and Sven Mattisson. On the use of mos varactors in rf vcos. *IEEE Solide-State Circuit*, 35(6), June 2000.

[20] J. Maget and M. Tiebout. Mos varactors with n- and p-type gates and their influence on an lc vco in digital cmo. *IEEE Solide-State Circuit*, 38(7), July 2003.

[21] A. Kral, F. Behbahani, and A. A. Abidi. Rf-cmos oscillators with switched tuning.

[22] Henrik Sjoland. Improved switched tuning of differential cmos vcos. *IEEE Transaction on Circuits and Systems-2: Analog and Digital Signal Processing*, 49(5), May 2002.

[23] H.T. Lin, Y.K. Chu, and H.R.Chuang. A 2 ghz, 0.25μm mos complementary vco with differential tuned mos varactor for wireless applications. Technical report, National Cheng Kung University, 2006.

[24] Ulrik Wismar, Dag Wisland, and Pietro Andreani. Linearity of bulk-controlled inverter ring vco in weak and strong inversion.

[25] Hong Zhang, Guican Chen, and Ning Li. A 2.4-ghz linear-tuning cmos lc voltage-controlled oscillator.

[26] A. Kral, F. Behbahani, and A.A. Abidi. Rf-cmos oscillators with switched tuning.

[27] Yoshiaki Yoshihara, Hirotaka Sugawara, Hiroyuki Ito, Kenichi Okada, and Kazuya Masu. Wide tuning range lc-vco using variable inductor for reconfigurable rf circuit. *IEICE TRAN. FUNDAMENTALS*, E88-A(2), February 2005.